New insights on the genesis of the Miocene collapse structures of the Island of Gozo (Malta, Central Mediterranean Sea)

J. P. Galve (1)*, C. Tonelli (2), F. Gutiérrez (3), S. Lugli (2), A. Vescogni (2) and M. Soldati (2)

(1) Departamento de Geodinámica, Universidad de Granada, Campus de Fuentenueva s/n, 18071 Granada, Spain; jpgalve@ugr.es (J.P.G.)

(2) Dipartimento di Scienze Chimiche e Geologiche, Università di Modena e Reggio Emilia, Largo S. Eufemia 19, 41121 Modena, Italy; chiara.tonelli@unimore.it (C.T.), stefano.lugli@unimore.it (S.L.), alessandro.vescogni@unimore.it (A.V.), soldati@unimore.it (M.S.)

(3) Departamento de Ciencias de la Tierra, Universidad de Zaragoza, C/Pedro Cerbuna 12, 50009 Zaragoza, Spain; fgutier@unizar.es (F.G.)

* Corresponding author's address: Departamento de Geodinámica, Universidad de Granada, Campus de Fuentenueva s/n, 18071 Granada, Spain.

E-mail: jpgalve@ugr.es (J.P.G.)

Tel.: +34 653 606226; Fax: +34 958 24 85 27.

Words of text: 6366

References: 80

Tables: 1

Figures: 11

Abbreviated title: Collapse structures of Gozo

Abstract

The large palaeosinkholes located in the NW of Gozo Island (Central Mediterranean Sea, Malta) offer excellent exposures that provide information on the geometry and kinematics of large karst-related collapse structures. Detailed geological analysis of these peculiar palaeosinkholes indicates that deep-seated evaporite dissolution is the most feasible hypothesis to explain their formation, according to the following evidence: (1) several structures have been formed by progressive foundering of cylindrical blocks with limited internal deformation as reveal the synsedimentary subsidence recorded by their Miocene sedimentary fill. This subsidence mechanism is more compatible with interstratal dissolution of evaporites than karstification and cave development in limestone formations. (2) The dimensions and deformation style of the palaeosinkholes are similar to those of other collapse structures related to deep-seated dissolution of salt-bearing evaporites. (3) The arcuate monocline associated with some of these collapse structures is also a characteristic feature of subsidence related to dissolution of evaporites. Notwithstanding, no major evaporite formations have been documented so far in the subsurface of the Malta Platform.

Supplementary material: Detailed descriptions of the collapse structures of the Island of Gozo (Malta, Central Mediterranean Sea) are available at www.geolsoc.org.uk/SUP00000.

Giant collapse sinkholes are one of the Earth's most dramatic and enigmatic landforms. Well-known examples include the Tiankengs of China and SE Asia, that reach several hundred meters deep and across (Waltham 2006), the Obruks of Central Anatolia (Bayari *et al.*, 2009), the large collapse dolines of the Dinaric karst (e.g. Velika Dolina, Waltham 2006; Crveno Jezero, Garašić 2000), and the Zacatón sinkhole in Mexico (Gary & Sharp 2006). Large collapse palaeosinkholes have been preserved in the geological record as gravitational deformation structures (e.g. ring faulting, breccia pipes) and related sedimentary features (e.g. sinkhole fills, local thickness variations, cumulative wedge-outs). These features have been described in the

Colorado Plateau, USA (Weir *et al.* 1961; Cater 1970; Sugiura & Kitcho 1981; Gutiérrez 2004), Southern Saskatchewan, Canada (Christiansen 1971; Gendzwill & Hajnal 1971; Christiansen and Sauer 2001), NE Spain (Gutiérrez 1996, 2014) and Southern Hunan, China (Min *et al.* 1997). Large collapse palaeosinkholes have also been identified through 3D seismic surveys in sedimentary basins of Southern Australia (Brown 1999), Venezuela (Castillo & Mann 2006), USA (McDonnell *et al*. 2007), Mediterranean Sea (Bertoni & Cartwright 2005, Lofi *et al*. 2012) and the South China Sea (Sun *et al*. 2013).

These structures have a multidisciplinary importance because their identification aids for ore and hydrocarbon exploration in sedimentary basins affected by deep-burial dissolution processes. Fossil collapse sinkholes are markers of large scale deep-seated karstification that favoured the migration and/or accumulation of hydrocarbons in the Maracaibo basin, Venezuela (Castillo & Mann 2006), in the Fort Worth basin, Texas, USA (McDonnell *et al*. 2007), and in the South China Sea basin (Sun *et al*. 2013). Palaeosinkhole-hosted uranium deposits of a high economic importance have been exploited in China (Min *et al*. 1997) and Arizona (USA) (Wenrich & Titley 2008). Sun *et al*. (2013) highlights that deep-burial dissolution should be taken into account when assessing reservoir heterogeneity and infrastructure risks in the largest offshore oil fields. This also applies to the evaluation and exploitation of ore deposits associated with palaeosinkholes. However, to our knowledge, studies on palaeosinkholes that may help to characterize deep-seated dissolution environments are very scarce. Detailed analyses on well-exposed large collapse structures, paying attention to their geometry, internal structure, kinematics and origin are needed to better understand similar structures and geomorphic features identified by indirect methods in the subsurface or in the sea floor.

The large palaeocollapse sinkholes of Gozo Island, Malta, central Mediterranean, described by Pedley (1974), are revisited in this paper. They offer excellent exposures that allow obtaining direct information on the internal architecture and kinematics of large karst-related collapse structures developed on the sea floor. In some cases, they display spectacular landforms of high

scientific and scenic value, which deserve protection and conservation measures (Coratza *et al.* 2012). Previous studies, dating back to the 1970s and 1980s, analyzed these fossil collapses from a sedimentological perspective (e.g. Pedley & Bennett 1985). Their main interest was that these paleosinkholes acted as sediment traps favouring the preferential accumulation of detrital phosphorites. Other aspects, such as their structural style and origin have not been analyzed in depth by previous authors, although Soldati *et al*. (2013) undertook a geomorphological study. Detailed examination and mapping of structural and stratigraphic features documented in this work, contribute to shed some light on their debatable origin. These large collapse features have been previously attributed to the breakdown of a cave system developed in limestone (Pedley 1974) or to deep-seated evaporite dissolution (Illies 1980; Pedley *et al.* 2002). The aim of this paper is to discuss these theories and the possible karstification and subsidence mechanisms responsible for their development. We have collected and analysed novel data regarding (1) regional geological and stratigraphic context; (2) stratigraphic and structural relationships observed in detailed geological maps; (3) stratigraphic and sedimentological features of the sediments deposited in the submarine sinkholes; (4) biostratigraphic data inferred from planktonic foraminifera; and (5) bathymetric data and geomorphological evidence of probable residual activity. This information allowed us to infer aspects related to the development of the sinkholes, including the deformation style, the spatial association with other structures of probable gravitational origin, the kinematics of the subsidence and its duration. The discussion on the possible genetic alternatives for the palaeosinkholes takes into account the new knowledge frame and a number of large dissolution-induced collapse structures documented worldwide.

Geological setting

The Maltese archipelago is located in the central Mediterranean Sea, around 90 km south of Sicily and 290 km east of Tunisia (Fig. 1A). It consists of three main islands: Malta (246 km^2), Gozo (67 km^2) and Comino (3.5 km^2) (Fig. 1B). From the geotectonic perspective, the archipelago is located in the northern African plate, and more specifically on the Pelagian

113 Platform, a continental shelf between southern Sicily (Malta-Ragusa platform) and northern
114 Libya (Tripolitanian platform) (Illies 1981) (Fig. 1A). These platforms constitute the foreland of
115 the south-verging Maghrebian Thrust Belt, at the collision zone between the Eurasian and
116 African plates. The Pelagian Platform is cut by the deep NW-SE trending trough of the
117 Pantelleria Rift. The northeastern part of the rift is designated as the Malta Graben (Gardiner *et*
118 *al.* 1995). The Maltese archipelago is located on the NE shoulder of the Pantelleria Rift, very
119 close to the master fault that controls the graben margin escarpment (Fig. 1A). Around 10 km
120 northwest of the Island of Gozo, there is an ENE-WSW-oriented graben, called the North Gozo
121 Graben. This structure is controlled by oblique dextral-normal faults that connect with the
122 normal faults of the Pantelleria Rift (tear faults). The kinematic evolution of these structures has
123 been inferred by Gardiner *et al.* (1995) on the basis of stratigraphic and structural relationships
124 observed in seismic profiles (e.g., thickness variations and offset sedimentary units). The
125 Pantelleria Rift began to open in late Miocene to mid-Pliocene time under an extensional
126 regime. The formation of the North Gozo Graben started in the late Pliocene, in relation with a
127 change in the tectonic regime, from simple extension to right-lateral transtension. The oblique
128 dextral faults with vertical components that control the North Gozo Graben offset in Pleistocene
129 sediments and the sea floor, strongly suggesting that they correspond to an active fault system
130 (Gardiner *et al.* 1995).
131
132 The rocks exposed in the islands comprise a Late Oligocene (Chattian) to Late Miocene
133 (Messinian) marine sedimentary succession mostly composed of limestones and marls (Fig.
134 1B). Five lithostratigraphic units form the outcropping sequence (Oil Exploration Directorate
135 1993; Pedley *et al.* 2002). The lowermost exposed unit is the *Lower Coralline Limestone*
136 *Formation* (Chattian) of pale-grey, hard, shallow marine biomicrites and biosparites around 140
137 m thick. The following units, in ascending order, are: (1) The *Globigerina Limestone Formation*
138 (Aquitanian-Langhian), a yellowish, fine-grained, planktonic foraminiferal limestone, 20 m to
139 over 200 m in thickness. This formation has been subdivided into three members by the
140 occurrence of laterally extensive phosphorite conglomerate beds; i.e. *Lower and Upper Main*

141 *Phosphorite Conglomerate Beds* (Pedley & Bennet 1985). (2) The *Blue Clay Formation*
142 (Serravallian-Tortonian) consists of grey, soft marls, clays and silty sands 20 to 70 m thick. (3)
143 The *Greensand Formation* (Tortonian) is brown and greenish glauconite-rich generally less
144 than 1 m thick, but reaching 11 m thick. (4) The *Upper Coralline Limestone Formation*
145 (Tortonian-Messinian) is broadly similar to the Lower Coralline Limestone Formation and up
146 to 160 m thick.
147
148 The unexposed stratigraphic units beneath the Late Oligocene Lower Coralline Limestone
149 Formation, were shown by the BP oil exploration borehole (Naxxar 2) on the Island of Malta
150 (Fig. 1B). It revealed a 3000 m thick sequence of platform carbonates, mainly dolomites, dating
151 back to the Lower Cretaceous in its lowermost part (Pedley 1990). Extensive dissolution-
152 related cavernisation was found within the Tertiary and Mesozoic carbonate strata in this
153 borehole (Pedley 1974). Another borehole drilled offshore by the Shell company (MS-A1
154 borehole; Fig. 1A) 40 km northeast of the Island of Malta shows a similar dolomite succession
155 5000 m thick down to the Lower Jurassic (Jongsma *et al.* 1985). The Madonna Taz-Zejt 1ST1
156 borehole, drilled on land in western Gozo (Fig. 1), proved a 3200 m thick Late Triassic
157 succession from a depth of 4.5 km, consisting of dolomites, shales and meters-thick anhydrite
158 beds, the latter with an aggregate thickness of ca. 230 m (Debono *et al.* 2000). In Zabbar and
159 Aqualta boreholes, drilled in the Malta Platform (Fig. 1A), a 1-m-thick gypsum bed has been
160 recorded at the Eocene-Oligocene boundary, 100-150 m below the base of the Lower Coralline
161 Limestone (Gatt & Gluyas 2012).
162
163 Overall, the geological structure of the Maltese archipelago is characterised by subhorizontal or
164 gently dipping Tertiary successions offset by different high-angle fault systems. The NW-SE-
165 trending Maghlaq Fault, on the southwestern edge of the Island of Malta (Fig. 1B), is the main
166 exposed normal fault related to the Pantelleria Rift, mostly located offshore to the southwest of
167 the archipelago (Illies 1980) (Fig. 1A). The general gentle NE dip of the Tertiary strata in the
168 archipelago is attributed to upwarping and backtilting on the NE shoulder of the Pantelleria Rift

(Illies 1980, 1981; Grasso & Pedley 1985). An ENE-WSW trending graben system around 15 km wide spans from southeastern Gozo to the central sector of Malta, including Comino Island and the straits between the three islands. This extensional structure, oblique with respect to the adjacent Pantelleria Rift, is bounded by the North Comino Channel Fault (or South Gozo Fault, of Grasso *et al.* 1986) to the north, and the Victoria Lines Fault to the south (Illies 1980) (Fig. 1B). The graben shows a concordant topography with a succession of flat-topped ridges (horsts) and valleys (grabens) controlled by ENE-WSW secondary normal faults. According to Gardiner *et al.* (1995), these originally normal faults may have reactivated as dextral strike-slip faults during the Plio-Pleistocene, concurrently with the development of the North Gozo Graben.

In the western sector of Gozo there is a system of E-W oblique-slip normal faults. Some of these faults offset vertically and laterally the annular collapse structures analysed in this work (Illies 1980, Oil Exploration Directorate 1993). Most probably, this fault system is related to the development of the adjacent North Gozo Graben since the late Pliocene, which shows evidence of recent faulting consistent with a right-lateral transtensional regime (Gardiner *et al.* 1995). This is a unique example in which dissolution collapse structures may be used as a structural marker to identify and assess neotectonic deformation.

Palaeosinkhole characteristics

The Island of Gozo has 13 mapped collapse palaeosinkholes controlled by subvertical dip-slip faults with circular to elliptical cartographic trace (Pedley 1974; Illies 1980; Oil Exploration Directorate 1993; Soldati *et al.* 2013) (Fig. 1B). We analysed, nine of the largest structures, mostly located in the western coastal sector of the island. Parameters including their size, geometry, amount of vertical displacement, subsurface dissolution and relative spatial distribution are shown in Table 1. Some palaeosinkholes reach exceptionally large dimensions ranging from 65 m to 600 m and most of them have a nearly circular geometry. The sizes of the palaeosinkholes generally decrease in area towards the northeast. The minimum vertical offset values range from >15 m to >60 m. The minimum cumulative dissolution volume for the eight

197 palaeosinkholes with data is 45.25 hm^3, roughly equivalent to a cube with an edge of 360 m.
198 The actual subsurface dissolution volumes may be substantially larger than the estimated ones
199 due to the following factors: (1) the structural throw used in the calculations is a minimum
200 value; (2) although strongly affected by dissolution, some stratigraphic levels may have not
201 collapsed; (3) the foundered sediments may have brecciated and increased their volume by
202 gravitational deformation due to the bulking effect (Gutiérrez & Cooper, 2013).
203
204 The Upper Coralline Limestone is the youngest stratigraphic unit affected by the collapse
205 structures. No deformed Quaternary deposits or landforms have been identified on land
206 associated with the faults bounding the palaeosinkholes. Quaternary stratigraphic and
207 geomorphic markers at the margins of the collapse structures are quite scarce. These data
208 suggest that at least some of the structures have been active sometime after the deposition of the
209 Late Miocene (Tortonian-Messinian) Upper Coralline Limestone, and that later they may have
210 been inactive or had a low subsidence rate.
211
212 Some collapses are offset by oblique-slip normal faults with strikes varying from ENE-WSW to
213 ESE-WNW. The subvertical collapse faults have been displaced horizontally by these tectonic
214 faults by as much as 46 m (Qawra palaeosinkhole) (Table 1). This evidence suggests that the
215 oblique-slip faults are younger than the gravitational collapse faults (post-Upper Coralline
216 Limestone). These oblique faults might still be active and are very probably related to the
217 formation of the ENE-WSW North Gozo Graben, which started in the Late Pliocene and shows
218 evidence of very recent activity (Gardiner *et al.* 1995).
219
220 Regarding the spatial distribution, the five palaeosinkholes in the western coastal sector of the
221 Island of Gozo are tightly clustered (Fig. 1B). The Xlendi and Tal Harrax structures, that have
222 elongated geometries and sharp changes in width, may correspond to the coalescence of
223 adjoining palaeosinkholes (Fig. 1B). Hereabouts, the development of the collapse structures
224 seems to have been controlled by NW-SE trending faults. The Dwejra North, Dwejra Bay and

225 Tal Harrax structures form a clear tightly-packed NW-SE alignment, and the major axis of the
226 latter elongated structure is oriented in the same direction (Fig. 2A). The rose diagram in Figure
227 2B shows the azimuth of the lines drawn between the centroid of each palaeosinkhole and its
228 nearest neighbour, plus the strikes of the faults mapped in the area. The lack of coincidence
229 between the prevalent NW-SE orientation inferred for the sinkholes and the strike of the tectonic
230 faults suggest that: (1) the development of the collapse structures may have been controlled by
231 NW-SE trending buried faults or joints with no cartographic expression; (2) the oblique-slip
232 faults that offset the whole Tertiary stratigraphic succession and the collapse structures may
233 have formed after the development of the palaeosinkholes.
234
235 Regarding the internal structure of the collapses, they are essentially downdropped blocks
236 bounded by steeply-dipping annular faults. Some structures seem to be controlled by a single
237 master ring fault (Il-Maxell, Xlendi, Qwara, Tal Harrax, Ghajn Abdul; Figs. 3, 4A, 5A and B,
238 6A and C, and 7) whereas others include nested failure planes with concentric (Qawra, Tal
239 Harrax, Dwejra Bay; Figs. 5A and C, 6A and 8) or exocentric arrangement (Dwejra North Bay;
240 Fig. 8). Small throw secondary faults (e.g., Il-Maxell, Xlendi and Qawra; Figs. 3, 4A and 5A)
241 and inward dips (e.g., Tal Harrax; Fig. 6B) are common in the periphery of the collapses.
242
243 The palaeosinkholes' infill shows the following characteristics (Pedley 1974; Pedley & Bennet
244 1985): (1) Some Miocene units are thicker in the collapsed blocks than in the surrounding areas
245 (Xlendi, Ghajn Abdul), and may also wedge out towards the rim of the palaeosinkholes (Il-
246 Maxell, Xlendi, Tal Harrax; Fig. 4C). (2) The strata in the collapsed plug typically display a
247 basin structure with centripetal dips (e.g., Xlendi, Tal Harrax, Ghajn Abdul; Figs. 4A, 6A and B,
248 and 7A). (3) The infill shows local changes in the depositional processes and facies. This is
249 clear in the cases of Xlendi (Fig. 4B and C) and Ghajn Abdul (Figs. 7C and 9A). (4) The
250 sediments of the palaeosinkhole fills abutting the marginal collapse faults may include
251 allochtonous blocks fallen from an adjacent submarine sinkhole scarp, which may be
252 accompanied by soft sediment deformation (Qawra, Tal Harrax, Ghajn Abdul; Figs. 5D, 6D and

9B).

The Dwejra area in western Gozo has a dramatic coastal landscape related to a cluster of four of the studied palaeosinkholes and represents an area of special interest (Figs. 1B and 10). These collapse structures are spatially associated with a peculiar monoclinal structure, already cited by Pedley & Bennet (1985). A structure-contour map of the top of the Lower Coralline Limestone has been constructed in order to characterise the fold (Fig. 10A). This is a west-facing semicircular monocline with centripetal dips and a maximum radius of about 900 m, which resemble half-a-structural basin. The lack of offshore data precludes elucidating whether the structure corresponds to a complete structural basin, or to a tightly curved down-to-the west monocline. The structural relief of the monocline, as indicated by the top of the Lower Coralline Limestone contour map, is around 60 m. The measured dips on the Tertiary strata are lower than 10° (or horizontal) in the upper and lower limbs, and exceed 15° in the dipping limb. Dwejra North palaeosinkhole, currently submerged by the sea, is located in the centre of the arcuate monocline, whereas Qwara, Tal-Harrax and Dwejra Bay palaeosinkholes partially overlap the dipping limb and/or the crest of the monocline (Fig. 10).

Discussion

The Island of Gozo shows unique examples of large collapse structures with dramatic geomorphic expression related to differential erosion controlled by the contrasting erodibility between the downdropped sediments and the surrounding bedrock (Soldati *et al*. 2013). These gravitational structures have been interpreted as dissolution-induced submarine palaeosinkholes that were active in the Miocene during the deposition of stratigraphic units overlying the Lower Coralline Limestone. Two hypotheses have been proposed to explain their genesis: (1) collapse of large caves developed within the Lower Coralline Limestone (Pedley 1974), and (2) deep-seated dissolution of halite-bearing evaporites and collapse of the overlying caprock sediments (Illies 1980).

281 According to Pedley's (1974) interpretation, the palaeosinkholes result from the collapse of
282 large caverns developed within the Lower Coralline Limestone. This author, inspired by the
283 "blue holes" of the Caribbean region, suggests that the cave systems formed during a probable
284 emergence phase in the Eocene or Oligocene period. Sea-level falls of ~50-60 m are reported in
285 the global sea-level curves at the Eocene-Oligocene boundary and in the Middle Oligocene
286 (Miller *et al.* 2011). Relative sea-level falls of 10 to 20 m are reported over Malta Platform in
287 the lower Chattian period by Gatt & Gluyas (2012). However, none appear to have been
288 sufficient to place western Gozo more than a few metres above sea-level.
289
290 Illies (1980) succinctly presented his evaporite dissolution interpretation without providing
291 much supporting data. Surprisingly, he used the oblique-slip faults that offset the
292 palaeosinkholes as diagnostic indicators of deep-seated salt dissolution and caprock collapse.
293 This highly questionable concept was based on the interpretation by Belderson *et al.* (1978) of
294 similar features recognized in the sea-floor of the eastern Mediterranean. According to these
295 authors, in their study area strike-slip faulting may have allowed sea water access to an
296 underlying salt layer triggering its dissolution. However, in our case study the oblique-slip faults
297 are superimposed on the paleocollapses, and consequently postdate them.
298
299 Below we discuss the origin of the Gozitan palaeosinkholes considering the available geological
300 data and analysing the similarities and differences with other large sinkholes and collapse
301 structures related to evaporite and carbonate dissolution documented worldwide, both onshore
302 and offshore.
303
304 *Subsidence kinematics and duration*
305 Overall, the available data indicate that the collapse process in the study area has operated over
306 a very long period of time in the late Cenozoic. The subsidence kinematics has probably been
307 dominated by progressive deformation, rather than by major episodes of gravitational faulting.
308 The study of the paleosinkholes infill provides multiple evidence of synsedimentary subsidence

309 in the sea-floor (Pedley 1974; Pedley & Bennet 1985): (1) Cumulative wedge-out arrangements
310 in the palaeosinkhole fill (Fig. 4C). (2) The boulders entombed in the latter indicate that there
311 were periods during which subsidence was not counterbalanced by aggradation (Figs. 5D, 6D
312 and 9B). (3) The depressions created by collapse subsidence in the sea floor controlled changes
313 in the depositional processes and facies. Moreover, in some palaeosinkholes synsedimentary
314 subsidence has been active over several periods. For instance, in Tal Harrax the available data
315 indicate that progressive subsidence has been active during deposition of the Globigerina
316 Limestone and the Blue Clay, probably spanning around 10 Ma in the Miocene (Fig. 6).
317 Stratigraphic evidence in Ghajn Abdul suggests that subsidence may have been active during
318 deposition of the Upper Coralline Limestone (Fig 7). Two collapse structures also record that
319 significant subsidence occurred after the sedimentation of the Upper Coralline Limestone
320 (Wardija Point, Wied il-Mielah; Fig. 11). Moreover, the nested enclosed depression 160 m
321 across and 4 m deep identified in the submerged floor of Dwejra North Bay suggests that some
322 collapses have been active in recent times (Fig. 8). Therefore, the analysed subsidence
323 phenomenon can be explained by progressive interstratal dissolution of soluble rocks at depth
324 over a very long time period, and the concomitant gradual collapse of the overlying formations.
325 These features related to the subsidence kinematics and duration seem to be more compatible
326 with interstratal dissolution of evaporites.
327
328 The stratigraphic relationships of the Crater Lake structure, and the Saskatoon low,
329 Saskatchewan, Canada, indicate that deep-seated salt dissolution and synsedimentary
330 subsidence have been active over several periods from the Late Cretaceous to the late
331 Pleistocene (Christiansen 1971; Christiansen & Sauer 2001). In the Delaware Basin, New
332 Mexico and Texas, USA, dissolution of Permian evaporites has generated depositional basins
333 filled with Neogene continental sediments that may reach 50 m in thickness (Hill 1996 and
334 references therein). Synsedimentary subsidence related to interstratal karstification of salt-
335 bearing evaporites has been also documented in a number of fluvial valleys, where Quaternary
336 alluvium shows substantial thickenings in dissolution basins (Guerrero *et al.* 2013 and

337 references therein; Gutiérrez & Cooper 2013). In contrast, the sedimentary fill in large sinkholes
338 related to the collapse of limestone caves commonly shows parallel-layered strata indicating that
339 subsidence has not been active during deposition. A good example of this is the Holocene fill of
340 the Blue Hole of Light House Reef, Belize, where there is no evidence of growth strata
341 (Gischler *et al.* 2013). This steep-sided submarine sinkhole 120 m deep and 320 m wide was
342 formed in the late Pleistocene by the collapse of a water table cave (White 1988). Features
343 indicative of synsedimentary subsidence have also been documented in limestone karst
344 sinkholes, although with notable differences with those observed in the Gozitan collapses. For
345 instance, in lakes of north-central Florida related to the coalescence of sinkholes, high-
346 resolution seismic data reveal geometrical relationships in the deposits indicative of
347 synsedimentary subsidence, but these are spatially and temporally restricted, and related mainly
348 to suffusion processes and dissolution at the rockhead (Kindinger *et al.* 1999).
349
350 *Dimensions and deformation style*
351 A striking feature of the studied palaeosinkholes is their gigantic dimensions. In the Maltese
352 Archipelago, cave systems have been developed in the Lower Coralline Limestone during
353 Quaternary sea-level lowstands, and locally roof breakdown has resulted in the development of
354 collapse sinkholes (Pedley 1974; Pedley *et al.* 2002). There are several significant onshore and
355 offshore examples. Il-Maqluba sinkhole in southern Malta is an elliptical depression 100 m long
356 with vertical cliffs 30 m high. There are also well-known submarine caves (e.g., Blue Dome, N
357 Gozo) and sinkholes (e.g., Blue Hole, Dwejra area, W Gozo, Fig. 10A), the latter up to 25 m
358 across and 15 m deep (Lemon 2012). However, the size of these collapses, as well as their
359 subsidence mechanism and kinematics, are very different from those of the Miocene
360 palaeosinkholes (Tonelli *et al.* 2012). These data indicate that large cavities exist within the
361 Lower Coralline Limestone, but they are most probably much younger than the Miocene
362 palaeosinkholes and not large enough to form tightly clustered collapses several hundred meters
363 across.
364

365 The largest documented caverns and collapse sinkholes associated with carbonate rocks occur in
366 inland mature karsts developed in massive limestones that have a high mechanical strength,
367 usually in humid tropical regions. The largest known cavern is Sarawak Chamber in Gunung
368 Mulu National Park, Malaysia. This underground void is 700 m long, 400 m wide and its vault-
369 shaped ceiling reaches around 100 m in height (Waltham 2004, 2006). The largest collapse
370 sinkholes are the Tiankengs described in China. These are giant sinkholes related to the collapse
371 of large chambers, commonly associated with substantial cave rivers (Waltham *et al.* 2005;
372 Xuewen & Waltham 2006). Xiaozhar Tiankeng, also known as the Heavenly Pit, is 628 m long
373 and 662 m deep. Deep collapse dolines have been also documented in the Dinaric karst, like
374 Crveno Jezero sinkhole, Croatia. This is a vertical-walled collapse around 500 m wide and more
375 than 530 deep, half submerged under a lake (Garašić 2000). However, it is not clear whether this
376 collapse structure is rooted in carbonate or evaporite rocks.
377
378 Although the size of the palaeosinkholes in Gozo is comparable with those of the
379 aforementioned carbonate karst landforms from China, there are significant differences
380 regarding the subsidence mechanism. The roof of large caverns developed in limestone typically
381 propagates upward through successive collapses controlled by arched failure planes. Ground
382 subsidence does not occur until the stopping process reaches the surface, leading to the
383 catastrophic formation of a collapse sinkhole. In contrast, as the stratigraphic record reveals,
384 subsidence has affected the sea-floor over millions of years, indicating long-sustained deep-
385 seated dissolution and sinkhole rejuvenation. In the analysed palaeosinkholes this subsidence
386 has been accommodated by the progressive foundering of cylindrical plugs with limited internal
387 deformation. This is clearly observable in the case of Qawra structure (Fig. 5). The
388 downdropped blocks bounded by steeply-dipping annular faults of the palaeosinkholes are
389 similar to those documented in volcanic calderas related to the slow decline of the supporting
390 magma. According to Roche *et al.* (2001), the foundering of this type of piston-like integral
391 blocks develops when the roof has an aspect ratio (roof thickness/roof width) within a specific
392 range, which depends on the mechanical properties of the rocks. This deformation style of the

393 palaeosinkholes of Gozo is very similar to the subsidence mechanism in other collapse
394 structures related to interstratal dissolution of salt-bearing evaporites described in the literature.
395 The Crater Lake depression, Saskatchewan, Canada, is a circular topographic basin underlain by
396 a downthrown cyclindrical block with two concentric fault zones 100 m and 200 m in diameter.
397 This collapse, with a vertical throw of 73 m, is related to interstratal dissolution of the halite-
398 bearing Middle Devonian Prairie Evaporite Formation, located at a depth of 914 m
399 (Christiansen 1971; Gendzwill & Hajnal 1971). The 45 km long structural basin of the
400 Saskatoon Low, Saskatchewan, Canada, is controlled by subvertical faults generated by
401 interstratal dissolution of Devonian salts, whose original thickness coincide with the maximum
402 throw of the structure (Christiansen 1967). This basin includes nested collapse structures
403 bounded by ring faults several kilometres in diameter (Christiansen & Sauer 2001). In the
404 Canyonlands section of the Colorado Plateau, USA, interstratal dissolution of evaporites in salt-
405 cored anticlines has produced collapse structures controlled by vertical failure planes with
406 circular and concentric forms. The downthrown blocks reach more than 500 m in diameter, are
407 rooted in evaporites at a depth of more than 600 m, and show vertical displacements up to 300
408 m (Weir *et al.* 1961; Cater 1970; Sugiura & Kitcho 1981; Gutiérrez 2004). In the Calatayud
409 Neogene Graben, Iberian Chain, NE Spain, interstratal karstification of halite- and glauberite-
410 bearing evaporites has generated collapses several kilometres across with a vertical
411 displacement of more than 200 m. Here the marginal faults of the collapse structures have an
412 irregular cartographic trace (Gutiérrez 1996, 2014).
413
414 Although the structure of the palaeosinkholes of Gozo have characteristics of deep-seated
415 collapses induced by interstratal evaporite dissolution, similar structures identified using 3D
416 seismic data have been attributed to the dissolution of carbonate rocks. Brown (1999)
417 recognized karst pits 200-500 m in diameter in deep burial Miocene carbonate rocks of the
418 Gippsland basin, southeastern Australia. Castillo and Mann (2006) identified subcircular
419 features up to 600 m wide and about 100 m deep in the Lower Cretaceous carbonates of the
420 Cogollo group in the southern Maracaibo Basin, Venezuela. These features were interpreted as

sinkholes formed subaerially by tropical weathering during a well-known eustatic drop in the sea level that occurred during the Aptian period in the Maracaibo region. In the northern Fort Worth Basin, Texas, McDonnell *et al.* (2007) identified subcircular collapse and sagging structures 500-2000 m in diameter that extend vertically for 760-1060 m. They explain these subsidence features as the coalescence of linked paleocaves in a limestone formation (Ellenburger Group) with incremental collapse of the overlying strata. In the northern South China Sea, 221 dissolution-collapse pipe structures 100-710 m wide and 134-1010 m deep were identified by Sun *et al.* (2013). In the Gulf of Lions, SW France, Lofi *et al.* (2012) used seismic profiles to image a subcircular collapse structure 2 km wide and 800 m deep with inward dipping concentric faults and an inner sagging structure. The authors attribute the genesis of the subsidence structures described in China and France to the collapse of limestone caves, although they do not have direct data on the soluble rock units at depth.

Spatial association with an arcuate monocline

The Dwejra palaeosinkhole cluster is spatially associated with a peculiar west-facing semicircular monocline suggesting a genetic link. The monocline has a radius of around 900 m and a structural relief of approximately 60 m. Monoclines related to the down-dip migration of dissolution fronts in evaporites and the consequent subsidence of the overlying strata (drape gravitational folding) have been documented in numerous regions; Saskatchewan, Canada. (Hopkins 1987; Anderson *et al.* 1988), NE England (Cooper 2002), southwest and central sectors of the USA (De Mille *et al.* 1964; Walters 1978; Anderson *et al.* 1994; Neal and Colpitts 1997; Gutiérrez *et al*. 2014), central Saudi Arabia (Powers *et al.* 1966; Memesh *et al.* 2008), Thailand (Supajanya and Friederich 1992), NE Spain (Gutiérrez *et al.* 2012a). Some of these dissolution-induced monoclines are accompanied by large caprock collapse sinkholes. In the Interior Homocline of central Saudi Arabia, dissolution of Late Jurassic anhydrite/gypsum units has generated a sinuous monocline more than 500 km long, locally affected by large caprock collapse sinkholes including Dahl Hit (Memesh *et al.* 2008; Gutiérrez & Cooper 2013). The sinkholes of Bottomless Lakes State Park, New Mexico, USA, are a sinuous chain of collapse

449 sinkholes that traverse a dissolution-induced monoclinal scarp on the eastern margin of the
450 Pecos River valley (Land 2003). The Holbrook Anticline in northern Arizona is a monocline
451 generated by interstratal dissolution of halite- and sylvite-bearing Permian evaporites at more
452 than 200 m depth. A number of active subsidence depressions 2-3 km across with nested
453 sinkholes (e.g., McCauley Sinks, Richard Lake) have been identified linked to this gravitational
454 drape fold (Neal *et al.* 2013; Conway & Cook 2013).
455
456 *Soluble rocks in the subsurface*
457 The available borehole data indicate the presence of very thick carbonate units with dissolution-
458 related cavern formation throughout the Tertiary and Mesozoic succession underlying the
459 Globigerina Limestone (Pedley 1974). In contrast, the reported evaporitic units are very deep or
460 have a limited thickness. The Late Triassic anhydrite beds recorded in Madonna Taz-Zejt 1ST1
461 borehole have a cumulative thickness of around 230 m, but occur below 4.5 km depth (Debono
462 *et al.* 2000). The relative shallow gypsum bed found 100-150 m below the base of the Lower
463 Coralline Limestone in the Malta Platform is just 1 m thick (Gatt & Gluyas 2012). These data
464 challenge the evaporite dissolution hypothesis. Dissolution-induced collapse structures around 1
465 km deep have been reported by several authors (e.g., Lu & Cooper 1996; McDonell *et al.* 2007;
466 Lofi *et al.* 2012), but to our knowledge, never as deep as 4.5 km. However, there is the
467 possibility that during the development of the palaeosinkholes in the Miocene, there were halite-
468 bearing evaporites that have been largely removed by dissolution. As Warren (2006) indicates, a
469 large proportion of the evaporitic formations deposited in the Earth's history have been largely
470 removed from the rock record by subsurface dissolution, and in many cases the only evidence of
471 their previous existence corresponds to frequently overlooked pointers of karstification such as
472 insoluble residues or breccias. The size of the palaeosinkholes in Gozo decreases towards the
473 NE. This spatial trend might be related to some kind of stratigraphic control, such as the
474 wedging out towards the NE of the soluble rock responsible for the collapse structures.
475
476 *Mechanism of karstification*

Large collapse sinkholes are usually formed in geological settings where buried evaporites are present (e.g., Paradox Valley and Delaware Basin, USA) or where large scale carbonate dissolution has occurred (e.g., China and Dinaric karst). Two main modes of large-scale carbonate dissolution have been documented in different karst settings: (1) karstification in a subaerial or shallow-burial environment by meteoric waters in humid regions and (2) deep-burial carbonate dissolution due to circulation of deep aggressive fluids. The first model cannot be invoked for the generation of the Maltese paleocollapses because of their deep-seated origin and evolution in a submerged environment. Several palaeosinkholes show syndepositional subsidence during the sedimentation of the Globigerina Limestone Formation. This formation records a long period spanning ca. 10 Ma (Aquitanian-Langhian) of sedimentation in the sea floor below the action of waves, interrupted by shallowing phases represented by hardgrounds and phosphorite conglomerate beds also formed below sea level (Pedley *et al* 2002; Föllmi *et al*. 2007).

Deep-burial carbonate dissolution can result from the circulation of corrosive fluids. The aggressiveness of these fluids on carbonate rocks may be enhanced by CO_2 (normally geothermal fluids) or H_2S (basinal fluids, connate waters) enrichments that are characteristics of active volcanic regions or areas adjacent to oil or gas fields (Ford & Williams, 2007).

Sinkholes and collapse structures related to CO_2 enriched geothermal fluids have been documented in numerous regions including; dissolution-collapse pipes in the South China Sea related to a magma intrusion (Sun *et al.* 2013), sinkholes of the Sistema Zacatón, Mexico (Gary & Sharp 2006), the Obrucks of central Anatolia, Turkey (Bayari *et al.* 2009), and collapse sinkholes of the San Vittorino Plain and Pontina Plain, Italy (Salvati & Sasowsky 2002). However, volcanic activity in the Maltese archipelago was restricted to the Jurassic (Patacca *et al.* 1979) and consequently it cannot be responsible for the Gozitan paleocollapses.

Large scale deep-burial carbonate dissolution may also be caused by acid pore waters resulting

505 from hydrocarbon degradation. Large caves have been formed due to this mechanism, including
506 the famous Carlsbad Caverns and Lechuguilla Cave, New Mexico. However, this alternative can
507 also be ruled out because, among other constraints, this process creates large caves at and
508 around the water table where the H_2S rising from depth mixes with O_2-rich meteoric waters
509 (Ford & Williams 2007). Therefore, it is not consistent with the submerged environment of
510 formation of the Gozitan palaeosinkholes.
511
512 The mixing of two fluids saturated in calcite may change the saturation state of the new
513 solution. According to Corbella & Ayora (2003) the mixing of two fluids in deep aquifers is
514 much more important for carbonate dissolution than the changes induced by the oxidation of
515 H_2S. According to their calculations, this is due purely to the mixing effect. No dissolution at the
516 scale of karst conduits would be expected by mixing two fluids with temperatures that differ
517 less than 10°C. Although these mechanism have been invoked to enhance porosity in deep
518 carbonate reservoirs, the modality and extent of karst features possibly formed by burial
519 carbonate dissolution are not well known and have been recently questioned by Ehrenberg *et al*.
520 (2012).
521
522 Conversely, evaporite dissolution in sub-sea burial environments is still poorly understood, but
523 it has been documented in the Eastern Mediterranean basin (Ross & Uchupi 1973; Kastens &
524 Spiess 1984; Bertoni & Cartwright 2005) and in the North Sea (Lohmann 1972; Jenyon 1983).
525 Thus, the mechanism of karstification associated with the Maltese palaeosinkholes may be
526 related to dissolution and removal of evaporites by sub-sea groundwaters. However, the
527 paleohydrogeological model responsible for the karstification of evaporites is difficult to
528 explain due to the shortage of data. A model involving groundwater discharge into the sea
529 cannot be invoked because the study area was an isolated carbonate platform when the Gozitan
530 palaeosinkholes started to form (Gatt & Gluyas 2012). A possible conceptual model adapted to
531 this situation is a subjacent dissolution related to focused vertical hydrothermal flow favoured
532 by seismic activity (*cf*. Bertoni & Cartwright 2005 for a detailed explanation). According to this

mechanism, the dissolution and subsidence that led to the development of the palaeosinkholes may be correlated to tectonically active periods, as reported by Gardiner *et al*. (1995), and not to sea level changes. This would explain why dissolution-induced subsidence is recorded by the Globigerina Limestone. Deposition of this formation was coeval to periods of activity on the ENE-WSW fault system (Pedley *et al.* 2002). The development of growth faults (Illies 1980) and the opening of Neptunian dykes (cracks formed in the sea floor into which sediment fell; Pedley *et al.* 2002), provide evidence of tectonic deformation affecting the sea floor. The current null, or very low, active subsidence in the palaeosinkholes may be attributed to a tectonic stabilization of the region and/or to the almost total dissolution of the evaporite horizons.

So far, the data available are quite limited to propose a robust hypothesis on the origin of the analysed palaeosinkholes. However, the data integrated in this work, together with the discussed points, provide a basis for future studies on the gigantic Gozitan paleosinkholes and collapse structures in other regions worldwide.

Conclusions

The detailed analysis of the well-exposed palaeosinkholes of Gozo Island provides novel insights into the geometry, internal structure, kinematics and origin of the collapse structures. The new knowledge frame, together with data from a number of large dissolution-induced collapse structures documented worldwide, suggest that deep-seated evaporite dissolution is the most satisfactory genetic hypothesis. This interpretation is supported by the following lines of evidence:

(1) The progressive foundering of cylindrical blocks with limited internal deformation over periods lasting of the order of 10 Ma. This indicates gradual removal of large volumes of evaporite rocks and the concomitant settlement of the overlying strata, rather than the development of large caverns and their upward propagation by stoping, characteristic of limestone karst.

(2) The dimensions and deformation style of the palaeosinkholes are similar to other collapse

structures related to interstratal dissolution of salt-bearing evaporites.

(3) The arcuate monocline associated with some of the studied paleosinkholes. This spatial association is commonly found in areas underlain by evaporitic formations affected by deep-seated dissolution.

Notwithstanding, no major evaporite beds have been documented so far in the subsurface stratigraphy of the Malta Platform. Future subsurface exploration (e.g., deep boreholes and geophysics), as well as petrological and geochemical analyses of Oligocene-Eocene carbonate units may provide new data on potential markers of dissolved evaporites or deep-burial carbonate dissolution. These studies and the examination of currently unaccesible exploration drillholes (e.g. Madonna Taz-Zejt well) might shed some light on the origin of these enigmatic structures and test the presented hypothesis.

The field activities were partially funded by a research project funded by the EUR-OPA Major Hazard Agreement of the Council of Europe (Responsible: M. Soldati). The work carried out by F. Gutiérrez has been partially supported by the Spanish national projects CGL2010-16775 and CGL2013-40867 (Ministerio de Economía y Competitividad). J.P. Galve would like to thank the Spanish Ministry of Economy and Competitiveness for his postdoctoral fellowship.

References

ABELS, H. A., HILGEN, F.J., KRIJGSMAN, W., KRUK, R.W., RAFFI, I., TURCO, E. & ZACHARIASSE, W.J. 2005. Long-period orbital control on middle Miocene global cooling: Integrated stratigraphy and astronomical tuning of the Blue Clay Formation on Malta. *Paleoceanography*, **20**, PA4012.

ANDERSON, N.L., BROWN, R.J. & HINDS, R.C. 1988. Geophysical aspects of Wabamun salt distribution in southern Alberta. *Canadian Journal of Exploration Geophysics*, **24**, 166–178.

ANDERSON, N.L., HOPKINS, J., MARTÍNEZ, A., KNAPP, R.W., MACFARLANE, P.A., WATNEY, W.L. & BLACK, R. 1994. Dissolution of bedded rock salt: a seismic profile across the active eastern margin of the Hutchinson salt member, central Kansas. *Computers and Geosciences*, **20**, 889–903.

BAYARI, C.S., PEKKAN, E. & OZYURT, N.N. 2009. Obruks, as giant collapse dolines caused by hypogenic karstification in central Anatolia, Turkey: Analysis of likely formation processes. *Hydrogeology Journal*, **17**, 327–345.

BELDERSON, R.H., KENYON, N.H. & STRIDE, A.H. 1978. Local submarine salt-karst formation on the Hellenic Outer Ridge , eastern Mediterranean. *Geology*, **6**, 716–720.

BERTONI, C. & CARTWRIGHT, J.A. 2005. 3D seismic analysis of circular evaporite dissolution structures , Eastern Mediterranean 3D seismic analysis of circular evaporite dissolution structures , Eastern Mediterranean. *Journal of the Geological Society*, **162**, 909–926.

BROWN, A.R. 1999. *Interpretation of Three-Dimensional Seismic Data. AAPG Memoir* 42.

CASTILLO, M.V. & MANN, P. 2006. Deeply buried, Early Cretaceous paleokarst terrane, southern Maracaibo Basin, Venezuela. *AAPG Bulletin*, **90**, 567–579.

CATER, F. 1970. *Geology of the Salt Anticline Region in Southwestern Colorado. U.S. Geological Survey Professional Paper 637*.

CHRISTIANSEN, E.A. 1967. Collapse structures near Saskatoon, Saskatchewan, Canada. *Canadian Journal of Earth Sciences*, **4**, 757–767.

CHRISTIANSEN, E.A. 1971. Geology of the Crater Lake Collapse Structure in Southeastern Saskatchewan. *Canadian Journal of Earth Sciences*, **8**, 1505–1513.

CHRISTIANSEN, E.A. & SAUER, E.K. 2001. Stratigraphy and structure of a Late Wisconsinan salt collapse in the Saskatoon Low , south of Saskatoon , Saskatchewan , Canada: an update. *Canadian Journal of Earth Sciences*, **1613**, 1601–1613.

CONWAY, B.D. & COOK, J.P. 2013. Monitoring evaporite karst activity and land subsidence in the Holbrook Basin, Arizona using interferometric synthetic aperture radar (InSAR). *In*: Land, L., Doctor, D. H. & Stephenson, J. B. (eds) *Sinkholes and the Engineering and Environmental Impacts of Karst. Proceedings of the Thirteenth Multidisciplinary Conference.* Carlsbad, New Mexico, National Cave and Karst Research Institute, 187–194.

COOPER, A.H. 2002. Halite karst geohazards (natural and man-made) in the United Kingdom. *Environmental Geology*, **42**, 505–512.

CORATZA, P., GALVE, J.P., SOLDATI, M. & TONELLI, C. 2012. Recognition and assessment of sinkholes as geosites: Lessons from the Island of Gozo (Malta). *Quaestiones Geographicae*, **31**, 25–35.

CORBELLA, M., AYORA, C., 2003. Role of fluid mixing in deep dissolution of carbonates. *Geologica Acta*, **1** (4), 305-313.

DE MILLE, G., SHOULDICE, J.R. & NELSON, H.W. 1964. Collapse structures related to evaporites of the Prairie Formation, Saskatchewan. *Geological Society of America Bulletin*, **75**, 307–316.

DEBONO, G., XERRI, S. & BISHOP, W.F. 2000. *Continental, Sabkha and Shallow Open Marine Liassic-Triassic Sequence Offers New Exploration Plays in Malta*. EAGE Conference on Geology and Petroleum Geology - St. Julians, Malta, 1 - 4 October 2000.

EHRENBERG, S. N.,1. WALDERHAUG, O, BJORLYKKE K., 2012. Carbonate porosity creation by mesogenetic dissolution: Reality or illusion? *AAPG Bulletin*, **96**, 217–233.

FÖLLMI, K.B., GERTSCH, B., RENEVEY, J.P., DE KAENEL, E. & STILLE, P. 2007. Stratigraphy and sedimentology of phosphate-rich sediments in Malta and south-eastern Sicily (latest Oligocene to early Late Miocene). *Sedimentology*, **55**, 1029–1051.

FORD, D. & WILLIAMS, P. 2007. *Karst Hydrogeology and Geomorphology*. Chichester, UK, John Wiley and Sons, Ltd.

GARAŠIĆ, P.M. 2000. Speloehydrologeological Research of Crveno jezero (Red Lake) near Imotski in Dinaric Karst Area (Croatia). *In*: *Proceedings of the Second Croatian Geological Congress*. Dubrovnik, Croatia, 587–590.

GARDINER, W., GRASSO, M. & SEDGELEY, D. 1995. Plio-pleistocene fault movement as evidence for mega-block kinematics within the Hyblean–Malta Plateau, Central Mediterranean. *Journal of Geodynamics*, **19**, 35–51.

GARY, M.O. & SHARP JR, J.M. 2006. Volcanogenic karstification of Sistema Zacatón , Mexico. *Geological Society of America Special Publication*, **404**, 79–89.

GATT, P.A. & GLUYAS, J.G. 2012. Climatic controls on facies in Palaeogene Mediterranean subtropical carbonate platforms. *Petroleum Geoscience*, **18**, 355–367.

GENDZWILL, D.J. & HAJNAL, Z. 1971. Seismic investigation of the Crater Lake collapse structure in southeastern Saskatchewan. *Canadian Journal of Earth Sciences*, **8**, 1514–1524.

GIANNELLI, L. & SALVATORINI, G. 1975. I Foraminiferi planctonici dei sedimenti terziari dell'Arcipelago maltese. I. Biostratigrafia di "Blue Clay", "Green Sands" a "Upper Globigerina Limestone. *Atti della Società Toscana di Scienze Naturali, Memorie ser. A 79*, 49–74.

GISCHLER, E., ANSELMETTI, F.S. & SHINN, E.A. 2013. Seismic stratigraphy of the Blue Hole (Lighthouse Reef , Belize), a late Holocene climate and storm archive. *Marine Geology*, **344**, 155–162.

GRASSO, M. & PEDLEY, H.M. 1985. The Pelagian Islands: a new geological interpretation from sedimentological and tectonic studies and its bearing on the evolution of the Central Mediterranean Sea (Pelagian Block). *Geologica Romana*, **24**, 13–34.

GRASSO, M., REUTHER, C.D., BAUMANN, H. & BECKER, A. 1986. Shallow crustal stress and neotectonic framework of the Malta Platform and the Southeastern Pantelleria Rift (Central Mediterranean). *Geol. Romana*, **25**, 191–212.

GUERRERO, J., GUTIÉRREZ, F. & GALVE, J.P. 2013. Large depressions, thickened terraces, and gravitational deformation in the Ebro River valley (Zaragoza area, NE Spain): Evidence of glauberite and halite interstratal karstification. *Geomorphology*, **196**, 162-176.

GUTIERREZ, F., CARBONEL, D., KIRKHAM, R.M., GUERRERO, J., LUCHA, P. & MATTHEWS, V. 2014. Can flexural-slip faults related to evaporite dissolution generate hazardous earthquakes? The case of the Grand Hogback monocline of west-central Colorado. *Geological Society of America Bulletin*, doi: 10.1130/B31054.1.

GUTIÉRREZ, F. 1996. Gypsum karstification induced subsidence: effects on alluvial systems and derived geohazards (Calatayud Graben, Iberian Range, Spain). *Geomorphology*, **16**, 277–293.

GUTIÉRREZ, F. 2004. Origin of the salt valleys in the Canyonlands section of the Colorado Plateau. *Geomorphology*, **57**, 423–435.

GUTIÉRREZ, F. 2014. Evaporite karst in Calatayud, Iberian Chain. *In*: *Landscapes and Landforms of Spain*. Dordrecht, Springer, 111–125.

GUTIÉRREZ, F. & COOPER, A.H. 2013. Surface Morphology of Gypsum Karst. *In*: *Treatise on Geomorphology, Volume 6, Karst Geomorphology*. San Diego, Elsevier, 425–437.

GUTIÉRREZ, F., CARBONEL, D., GUERRERO, J., MCCALPIN, J.P., LINARES, R., ROQUÉ, C. & ZARROCA, M. 2012a. Late Holocene episodic displacement on fault scarps related to interstratal dissolution of evaporites (Teruel Neogene Graben, NE Spain). *Journal of Structural Geology*, **34**, 2–19.

HILL, C. 1996. *Geology of the Delaware Basin, Guadalupe, Apache, and Glass Mountains, New Mexico and West Texas. Permian Basin Section-SEPM, Publication No. 96-39*.

HOPKINS, J.C. 1987. Contemporaneous subsidence and fluvial channel sedimentation: Upper Mannville C Pool, Berry Field, Lower Cretaceous of Alberta. *The American Association of Petroleum Geologists Bulletin*, **71**, 334–345.

ILLIES, J.H. 1980. Form and function of graben structures: the Maltese Islands. *In*: Cloos, H., Ghelen, K., Illies, J. H., Kuntz, E., Neumann, J. & Seibold, E. (eds) *Mobile Earth*. Boppard, Boldt, 161–184.

ILLIES, J.H. 1981. Graben formation–the Maltese Islands–a case history. *Tectonophysics*, **73**, 151–168.

JENYON, M.K. 1983. Seismic response to collapse structures in the Southern North Sea. *Marine and petroleum Geology*, **1**, 27–36.

JONGSMA, D., VAN HINTE, J.E. & WOODSIDE, J.M. 1985. Geologic structure and neotectonics of the North African continental margin south of Sicily. *Marine and petroleum Geology*, **2**, 156–179.

KASTENS, K.A. & SPIESS, F.N. 1984. Dissolution and collapse features on the Eastern Mediterranean Ridge. *Marine Geology*, **56**, 181–193.

KINDINGER, J.L., DAVIS, J.B. & FLOCKS, J.G. 1999. Geology and evolution of lakes in. *Environmental Geology*, **38**, 301–321.

LAND, L. 2003. Evaporite karst and regional ground water circulation in the lower Pecos Valley. *In*: Johnson, K. H. & Neal, J. T. (eds) *Evaporite Karst and Engineering/environmental Problems in the United States. Oklahoma Geological Survey Circular. 109*. Oklahoma Geological Survey, 227–232.

LEMON, P.G. 2012. *Scuba Diving Malta Gozo Comino – The Ultimate Guide to Diving the Maltese Islands*, *3rd Edition*. Peter G. Lemon.

LOFI, J., BERNÉ, S., TESSON, M., SERANNE, M. & PEZARD, P. 2012. Giant solution-subsidence structure in the Western Mediterranean related to deep substratum dissolution. *Terra Nova*, **24**, 181–188.

LOHMANN, H.H. 1972. Salt dissolution in subsurface of British North Sea as interpreted from seismograms. *AAPG Bulletin*, **56**, 472–479.

LU YAORU & COOPER, A.H. 1996. Gypsum karst in China. *International Journal of Speleology*, **25**, 297–307.

MCDONNELL, A., LOUCKS, R.G. & DOOLEY, T. 2007. Quantifying the origin and geometry of circular sag structures in northern Fort Worth Basin , Texas : Paleocave collapse , pull-apart fault systems , or hydrothermal alteration? *AAPG Bulletin*, **9**, 1295–1318.

MEMESH, A., DINI, S., GUTIÉRREZ, F. & WALLACE, C.A. 2008. Evidence of large-scale subsidence caused by interstratal karstification of evaporites in the Interior Homocline of Central Saudi Arabia. *Geophysical Research Abstracts*, A–02276.

MILLER, K.G., MOUNTAIN, G.S., WRIGHT, J.D. & BROWNING, J.V. 2011. A 180-million-year record of sea level and ice volume variations from continental margin and deep-sea isotopic records. *Oceanography*, **24**, 40–53.

MIN, M., ZHENG, D., SHEN, B., WEN, G., WANG, X. & GANDHI, S.S. 1997. Genesis of the Sanbaqi deposit: a paleokarst-hosted uranium deposit in China. *Mineralium Deposita*, **32**, 505–519.

742 NEAL, J.T. & COLPITTS, R.M. 1997. Richard Lake, an evaporite karst depression in the
743 Holbrook Basin, Arizona. *Carbonates and Evaporites*, **12**, 91–98.

744 NEAL, J.T., JOHNSON, K.S. & LINDBERG, P. 2013. Variations in evaporite karst in the
745 Holbrook Basin, Arizona. *In*: Land, L., Doctor, D. H. & Stephenson, J. B. (eds)
746 *Sinkholes and the Engineering and Environmental Impacts of Karst. Proceedings*
747 *of the Thirteenth Multidisciplinary Conference.* Carlsbad, New Mexico, National
748 Cave and Karst Research Institute, 177–186.

749 OIL EXPLORATION DIRECTORATE. 1993. Geological map of the Maltese Islands.

750 PATACCA, E., SCANDONE, P., GIUNTA, G. & LIGUORI, V. 1979. Mesozoic paleotectonic
751 evolution of the Ragusa Zone (SE Sicily). *Geologica Romana*, **18**, 331–369.

752 PEDLEY, H.M. 1974. Miocene sea-floor subsidence and later subaerial solution
753 subsidence structures in the Maltese Islands. *Proceedings of the Geologists'*
754 *Association*, **85**, 533–547.

755 PEDLEY, H.M. 1990. Syndepositional tectonics affecting Cenozoic and Mesozoic
756 deposition in the Malta and SE Sicily areas (Central Mediterranean) and their
757 bearing on Mesozoic reservoir development in the N Malta offshore region.
758 *Marine and petroleum geology*, **7**, 171–180.

759 PEDLEY, H.M. & BENNET, S.M. 1985. Phosphorites, hardgrounds and syndepositional
760 solution subsidence: A palaeoenvironmental model from the Miocene of the
761 Maltese islands. *Sedimentary Geology*, **45**, 1–34.

762 PEDLEY, H.M., CLARKE, M.H. & GALEA, P. 2002. *Limestone Isles in a Crystal Sea: The*
763 *Geology of the Maltese Islands.* Valletta, Malta, Malta: Publishers Enterprises
764 Group.

765 POWERS, R.W., RAMIREZ, L.F., REDMOND, C.D. & ELBERG JR., E.L. 1966. *Geology of*
766 *the Arabian Peninsula; Sedimentary Geology of Saudi Arabia. U.S. Geological*
767 *Survey Professional Paper 560-D*.

768 ROCHE, O., VAN WYK DE VRIES, B. & DRUITT, T.H. 2001. Sub-surface structures and
769 collapse mechanisms of summit pit craters. *Journal of Volcanology and*
770 *Geothermal Research*, **105**, 1–18.

771 ROSS, D.A. & UCHUPI, E. 1973. Structure and sedimentary history of Southeastern
772 Mediterranean Sea–Nile Cone Area. *AAPG Bulletin*, **61**, 872–902.

773 SALVATI, R. & SASOWSKY, I.R. 2002. Development of collapse sinkholes in areas of
774 groundwater discharge. *Journal of Hydrology*, **264**, 1–11.

775 SOLDATI, M., TONELLI, C. & GALVE, J.P. 2013. Geomorphological evolution of
776 palaeosinkhole features in the Maltese archipelago (Mediterranean Sea). *Geografia*
777 *Fisica e Dinamica Quaternaria*, **36**, 189–198.

778 SUGIURA, R. & KITCHO, C.A. 1981. Collapse structures in the Paradox Basin. *In*:
779 *Geology of the Paradox Basin*. Denver, Colorado, USA, Rocky Mountain
780 Association of Geologists, 33–45.

781 SUN, Q., CARTWRIGHT, J., WU, S. & CHEN, D. 2013. 3D seismic interpretation of
782 dissolution pipes in the South China Sea: Genesis by subsurface, fluid induced
783 collapse. *Marine Geology*, **337**, 171–181.

784 SUPAJANYA, T. & FRIEDERICH, M.C. 1992. Salt tectonics of the Sakon Nakhon Basin,
785 norhteastern Thailand. *In*: *Seventh Regional Conference on Geology, Mineral and*
786 *Hydrocarbon Resources of Southeast Asia (GEOSEA VII)*.

787 TONELLI, C., GALVE, J.P., CALLEJA, I. & SOLDATI, M. 2012. Spatial analysis of
788 sinkholes as a tool to understand the karst sytem evolution. A case study from the
789 Maltese archipelago. *In*: Scappini, S. & Zapparoli, S. (eds) *Proceedings of the 7th*
790 *European Congress on Regional Geoscientific Cartography and Information*
791 *Systems - Bologna, Italy, 12th-15th June 2012*. Regione Emilia-Romagna, 243–
792 244.

793 WALTERS, R.F. 1978. *Land Subsidence in Central Kansas Related to Salt Dissolution,*
794 *Vol. 214*. University of Kansas Publications.

795 WALTHAM, T. 2004. Mulu, Sarawak. *In*: Gunn, J. (ed.) *Encyclopedia of Caves and*
796 *Karst Science*. Fitzroy Dearborn, 531–533.

797 WALTHAM, T. 2006. Tiankengs of the world , outside China. *Speleogenesis and*
798 *Evolution of Karst Aquifers*, **4**, 1–12.

799 WALTHAM, T., BELL, F. & CULSHAW, M. 2005. *Sinkholes and Subsidence*. Chichester,
800 UK, Praxis Publishing.

801 WARREN, J.K. 2006. *Evaporites. Sediments, Resources and Hydrocarbons*. Berlin,
802 Springer.

803 WEIR, G.W., PUFFETT, W.P. & DODSON, C.L. 1961. Collapse structures of southern
804 Spanish Valley, Southeastern Utah. U.S. Geological Survey Professional Paper
805 424-B. 173–175.

806 WENRICH, K.J. & TITLEY, S.R. 2008. Uranium exploration for northern Arizona (USA)
807 breccia pipes in the 21st century and consideration of genetic models. *In*: Spencer,
808 J. E. & Titley, S. R. (eds) *Ores and Orogenesis: Circum-Pacific Tectonics,*
809 *Geologic Evolution, and Ore Deposits: Arizona Geological Society Digest 22*.
810 295–309.

811 WHITE, W.B. 1988. *Geomorphology and Hydrology of Karst Terrains*. Oxford, U.K.,
812 Oxford Univ. Press.

813 XUEWEN, Z. & WALTHAM, T. 2006. Tiankeng: definition and description. *Speleogenesis*
814 *and Evolution of Karst Aquifers*, **4**, 1–8.

815

Tables

Table 1. *Parameters related to the size, geometry, amount of vertical displacement, subsurface dissolution volume, relative spatial distribution and geomorphic expression of the nine selected palaeosinkholes of western Gozo (note 1hm^3 is 1,000,000 m^3).*

Palaeosinkhole name	Major axis (m)	Minor axis (m)	Elongation ratio	Area (m^2)	Throw (m)	Volume of dissolved karst rocks (hm^3)	Youngest sediments displaced	Distance to the nearest collapse (m)	Horizontal offset on cross-cutting tectonic faults (m)	Geomorphic expression
Qawra	368	365	1.01	110,085	>60	>6.61	Blue Clay	75	46	depression
Tal Harrax	596	556	1.07	325,064	~100	>16.25	Blue Clay	30	16	depression
Xlendi	330	278	1.19	112,171	>50	>6.17	Globigerina Limestone	1,600		depression
Dwejra North	337	311	1.08	82,088	>40	>3.28	Globigerina Limestone?	38	/	bay
Dwejra Bay	380	351	1.08	120,762	>40	>4.83	Globigerina Limestone?	30	16	bay
Il-Maxell	>120	>120	?	?	>15	?	Globigerina Limestone	1,290	/	depression
Ghajn Abdul	440	371	1.18	130,575	>50	>6.53	Upper Coralline Limestone	550		mesa
Wardija Point	65	48	1.35	2,497	>50	>0.12	Upper Coralline Limestone	845	/	butte
Wied il-Mielah	181	176	1.03	24,389	>60	>1.46	Upper Coralline Limestone	2,180	/	butte

Figure captions

Fig. 1. (**A**) Sketch showing the geotectonic setting of the Maltese archipelago, and the main deep boreholes drilled in and around the islands. (**B**) Simplified geological map of the Maltese archipelago showing the distribution of stratigraphic units and faults, as well as the palaeosinkholes of Gozo Island. On the right, close up of the NW sector of Gozo indicating the name of the collapse structures analysed in this work.

Fig. 2. (**A**) Sketch of the western sector of Gozo Island showing the NW-SE prevalent distribution of the palaeosinkholes. (**B**) Rose diagram representing azimuth of the lines between the centroid of each palaeosinkhole and that of the nearest one (black color) and the strike of the faults mapped in the western sector of Gozo (grey color). The dashed circle corresponds to one measurement.

Fig. 3. The Il-Maxell palaeosinkhole. A: Main NW-SE-oriented exposure showing the western edge of the collapse structure controlled by arcuate master and secondary faults. B: Northern side of the exposure and sketch. C: Southern exposure with sketch. The Il-Maxell structure is the only palaeosinkhole of Gozo in which it is possible to observe the deformation style in the sediments underlying the depression fill, a mosaic packbreccia (Warren 2006), largely consisting of meter-sized slab-like blocks of fragmented and dislocated tabular beds.

Fig. 4. (**A**) Detailed geological map and cross-section of the Xlendi palaeosinkhole, offset by oblique dextral-normal tectonic faults. Several small throw radially disposed dip-slip faults in the structure affect the sinkhole infill. (**B**) General view of the Xlendi collapse from the south. (**C**) Cumulative wedge-out and progressive upward dip attenuation in the Globigerina Limestone strata of the palaeosinkhole fill (NE margin).

Fig. 5. (**A**) Detailed geological map of the Qawra palaeosinkhole. Most of the collapse depression is underlain by the Blue Clay, largely masked by vegetation, but where exposed these sediments show an undisturbed dominant subhorizontal structure. Two samples were collected from this stratigraphic unit for planktonic foraminifera assemblage biostratigraphy (the asterisk indicate the location of samples). The lower sample contained *Paragloborotalia siakensis*, *Dentoglobigerina altispira* and *Globigerinoides* spp. The upper one had more and better developed *P. siakensis* and scarce *Paragloborotalia partimlabiata*. According to Abels *et al*. (2005), the first occurrence of *P. partimlabiata* is found in the upper part of the Blue Clay suggesting that the exposed sediments correspond to the middle and upper sections of the Blue Clay (**B**) View of the NE sector of the erosional depression excavated within the palaeosinkhole. The steep scarp on Lower Coralline Limestone corresponds to the exhumed rim fault of the collapse structure. The vegetated slopes at the foot of the scarp are underlain by softer Blue Clay and Upper Globigerina Limestone. The lagoon is connected to the sea through a fault controlled cave. (**C**) Southeast margin of the collapse, where Upper Globigerina Limestone (vegetated slope) is juxtaposed to Lower Coralline Limestone (bare rock exposure). (**D**) Boulder of reworked Lower Globigerina Limestone incorporated within the Upper Globigerina deposited in the palaeosinkhole. The boulder is interpreted as a block fallen from the scarped margin of the submarine sinkhole in Miocene time. LC: Lower Coralline Limestone; LG: Lower Globigerina Limestone; UG: Upper Globigerina Limestone.

Fig. 6. (**A**) Detailed geological map of the Tal Harrax palaeosinkhole. (**B**) Sagging strata of Upper Globigerina Limestone at the southernmost sector of Tal Harrax depression. (**C**) Tal Harrax rim fault outcrop. LC: Lower Coralline Limestone; LG: Lower Globigerina Limestone. (**D**) Boulders of Globigerina Limestone (GL) entombed within Blue Clay (BC) deposits at the centre of Tal Harrax structure. This Blue Clay outcrop contains a high detrital fraction, including abundant glauconite clasts, suggesting that it may correspond to the upper part of the formation, close to the contact with the Greensand Formation (Giannelli & Salvatorini 1975). This interpretation is supported by the planktonic foraminifera assemblage in two samples collected for this investigation (*P. siakensis*, *P. partimlabiata* and *Globorotalia menardii)*.

Fig. 7. Detailed geological map of the Ghajn Abdul palaeosinkhole (**A**) and cross-section (**B**). The numbers in the geological map indicate the stratigraphic sections shown in C. (**C**) Stratigraphic sections recorded in Ghajn Abdul palaeosinkhole (1, 2 and 3) and in the adjacent mesa.

Fig. 8. Digital elevation model generated from LiDAR data, showing the topography of the sea floor at Dwejra North Bay and Dwejra Bay. Note the steep-sided enclosed depression in the NE sector of the bay controlled by the collapse structure. The bottom of the closed depression has a marginal trough and a protruding central sector with blocky appearance.

Fig. 9. (**A**) Upper part of Ghajn Abdul mesa capped by Upper Coralline Limestone. Note the low-angle cross stratified packstones and grainstones overlain by bioturbated massive limestone at the top. (**B**) Load casts and contorted bedding in the cross stratified packstones and grainstones associated with large meter-sized allochtonous boulders of grainstones containing pectinids, echinoderms, oysters and gastropods.

Fig. 10. (**A**) Structure contour map of the top of the Lower Coralline Limestone illustrating the arcuate west-facing monoclinal structure of Dwejra area. (**B**) General view of the west sector of the monocline from the sea. (**C**) Detail of the attitude of the strata at Fungus Rock.

Fig. 11. Aerial orthoimages of Wied il-Mielah (**A**) and Wardija Point (**B**) palaeosinkholes. The cartographic relationships observed in these structures indicate that the collapses were active after the deposition of the Upper Coralline Limestone in Pliocene and probably Quaternary times. UCL: Upper Coralline Limestone; GL: Globigerina Limestone.

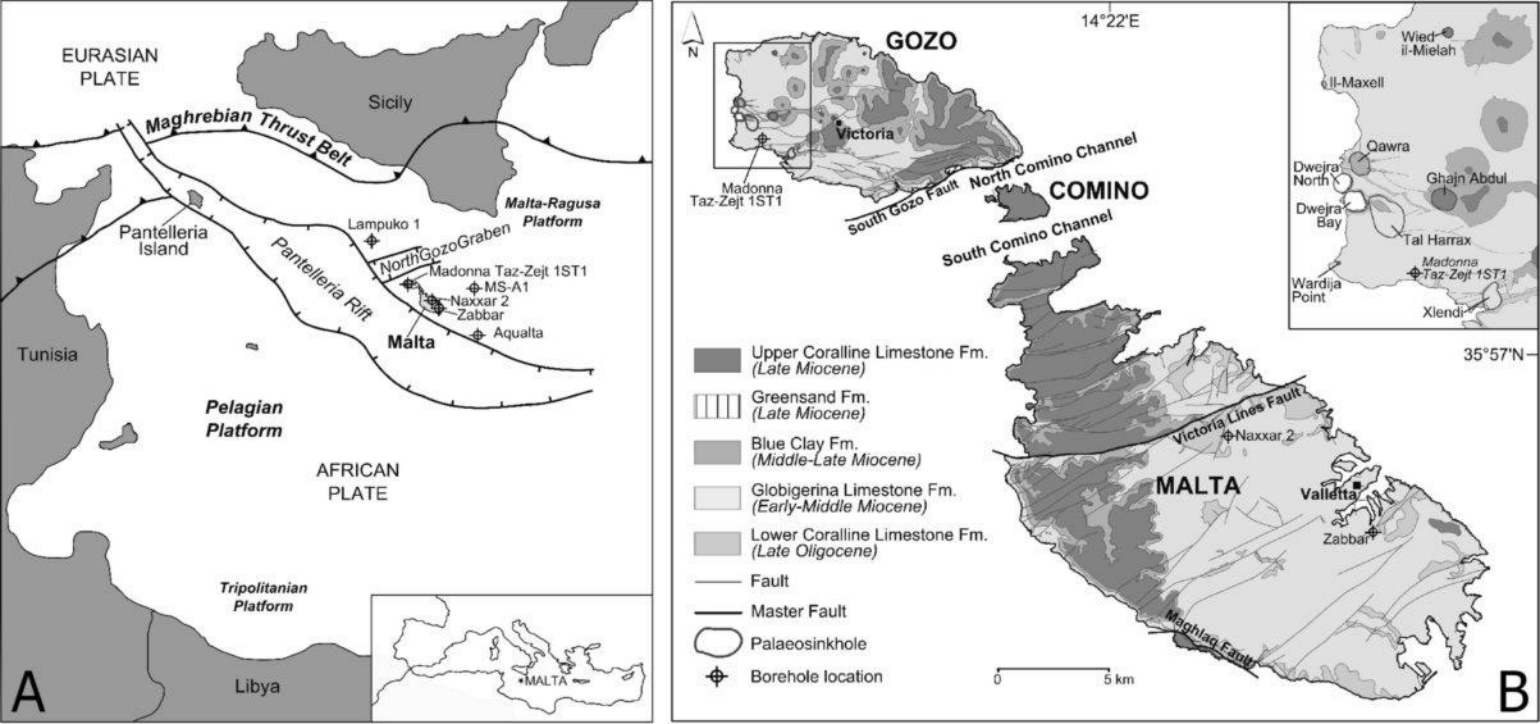
EURASIAN PLATE
Sicily
Maghrebian Thrust Belt
Malta-Ragusa Platform
Pantelleria Island
Lampuko 1
North Gozo Graben
Madonna Taz-Zejt 1ST1
MS-A1
Naxxar 2
Zabbar
Aqualta
Pantelleria Rift
Malta
Tunisia
Pelagian Platform
AFRICAN PLATE
Tripolitanian Platform
Libya
MALTA
A
GOZO
14°22'E
N
Victoria
Madonna Taz-Zejt 1ST1
North Comino Channel
South Gozo Fault
COMINO
South Comino Channel
Wied il-Mielah
il-Maxell
Qawra
Dwejra North
Ghajn Abdul
Dwejra Bay
Tal Harrax
Madonna Taz-Zejt 1ST1
Wardija Point
Xlendi
35°57'N
Upper Coralline Limestone Fm. (Late Miocene)
Greensand Fm. (Late Miocene)
Blue Clay Fm. (Middle-Late Miocene)
Globigerina Limestone Fm. (Early-Middle Miocene)
Lower Coralline Limestone Fm. (Late Oligocene)
Fault
Master Fault
Palaeosinkhole
Borehole location
Victoria Lines Fault
Naxxar 2
MALTA
Valletta
Zabbar
Maghlaq Fault
0
5 km
B

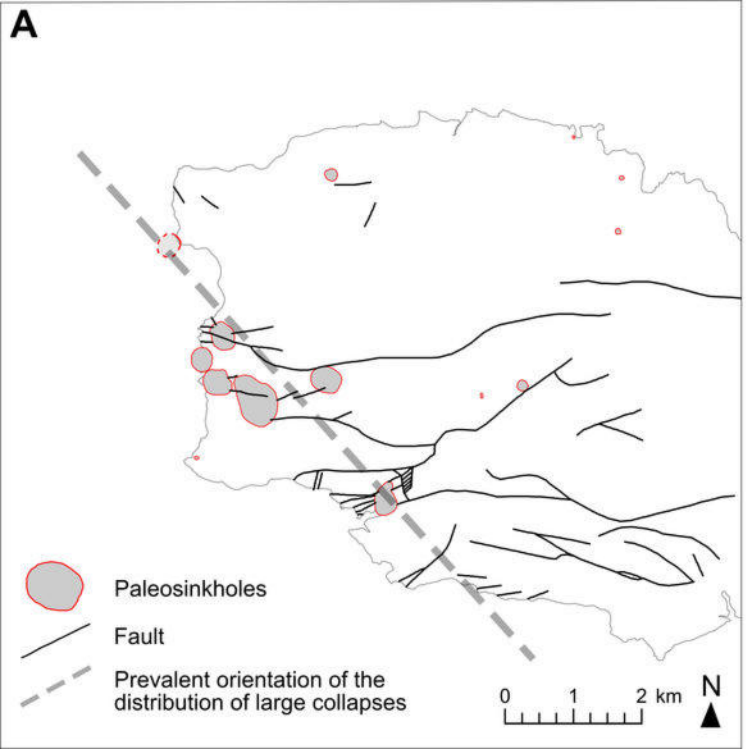
A
Paleosinkholes
Fault
Prevalent orientation of the distribution of large collapses
0 1 2 km
N

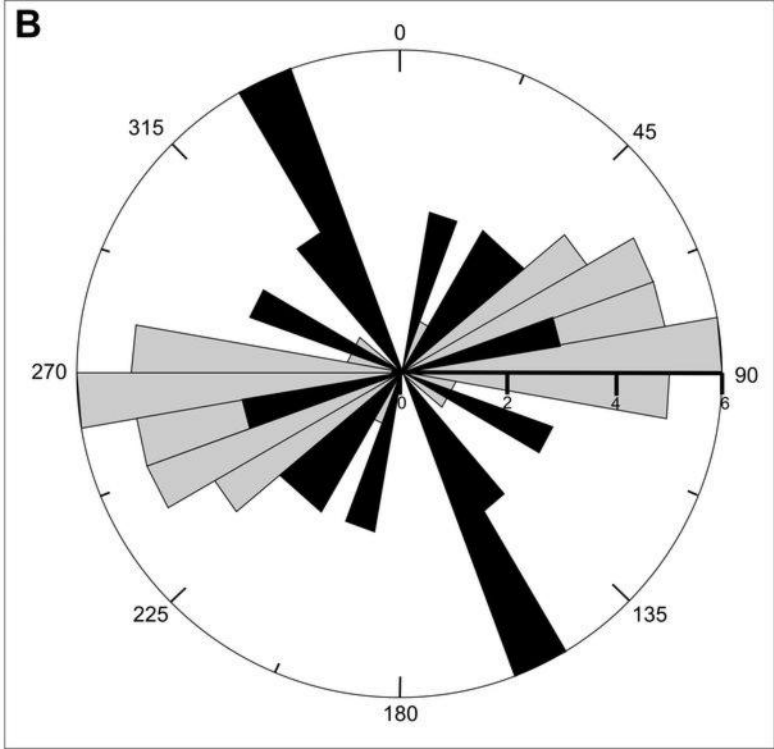
B
0
45
90
135
180
225
270
315
0
2
4
6

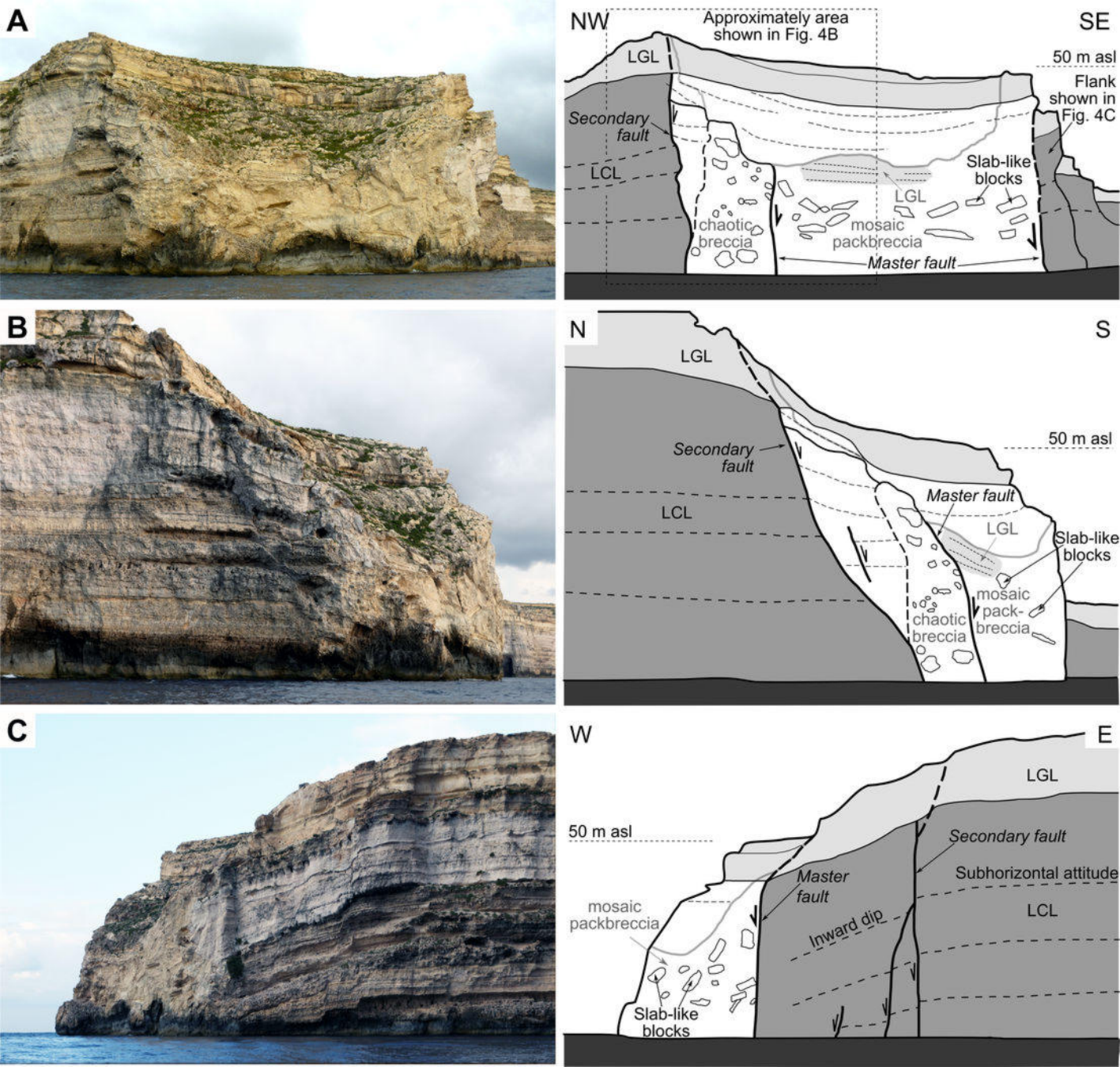
A
NW
Approximately area shown in Fig. 4B
SE
LGL
50 m asl
Flank shown in Fig. 4C
Secondary fault
LCL
Slab-like blocks
LGL
chaotic breccia
mosaic packbreccia
Master fault
B
N
S
LGL
50 m asl
Secondary fault
Master fault
LCL
LGL
Slab-like blocks
mosaic pack-breccia
chaotic breccia
C
W
E
LGL
50 m asl
Secondary fault
Subhorizontal attitude
Master fault
mosaic packbreccia
LCL
Inward dip
Slab-like blocks

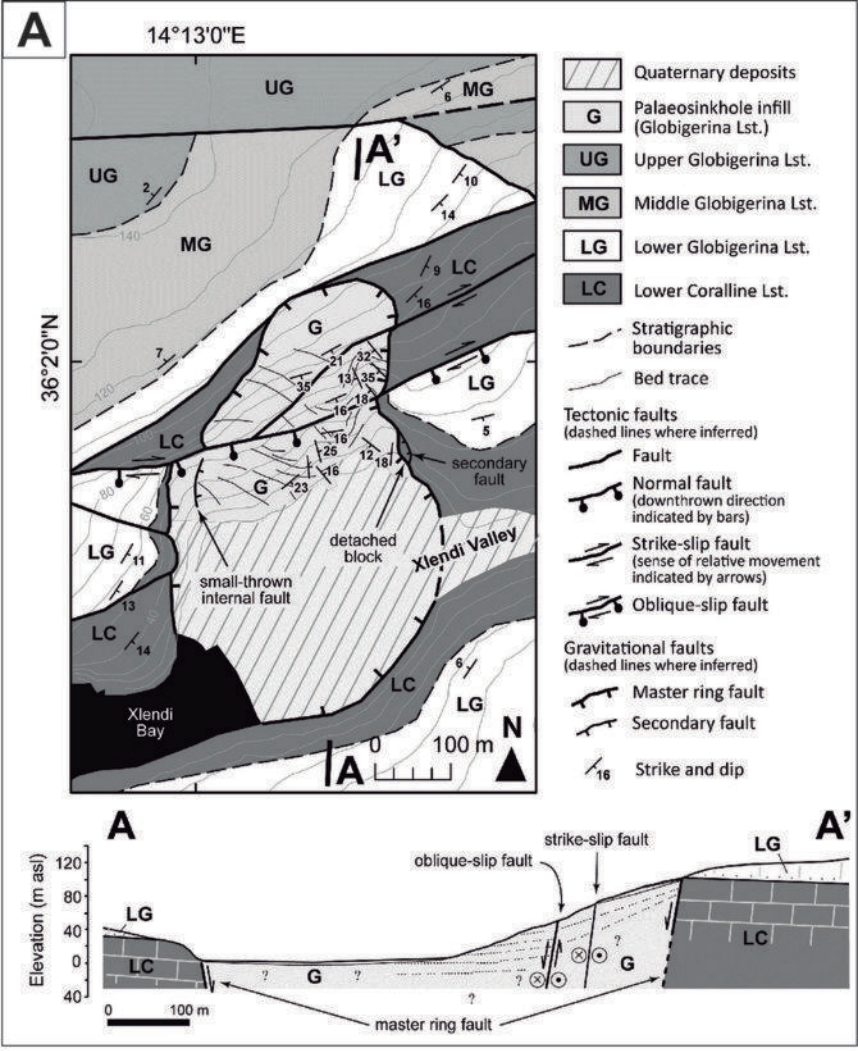
A
14°13'0"E
36°2'0"N
UG
MG
LG
LC
G
A'
secondary fault
detached block
Xlendi Valley
small-thrown internal fault
Xlendi Bay
0 100 m
N
Quaternary deposits
Palaeosinkhole infill (Globigerina Lst.)
Upper Globigerina Lst.
Middle Globigerina Lst.
Lower Globigerina Lst.
Lower Coralline Lst.
Stratigraphic boundaries
Bed trace
Tectonic faults
(dashed lines where inferred)
Fault
Normal fault
(downthrown direction indicated by bars)
Strike-slip fault
(sense of relative movement indicated by arrows)
Oblique-slip fault
Gravitational faults
(dashed lines where inferred)
Master ring fault
Secondary fault
Strike and dip
A
A'
Elevation (m asl)
120
80
40
0
40
oblique-slip fault
strike-slip fault
master ring fault
0 100 m

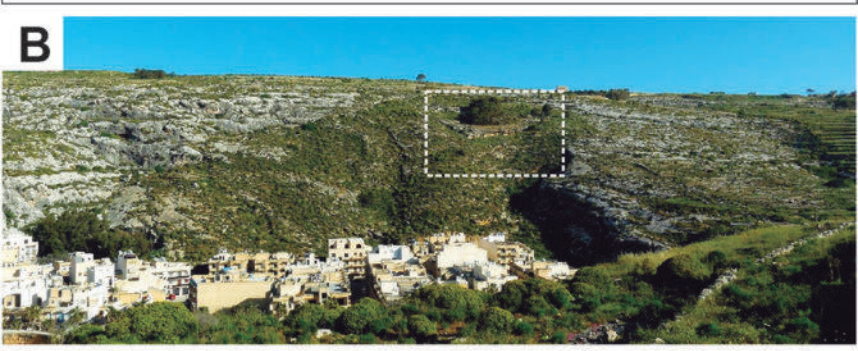
B


C

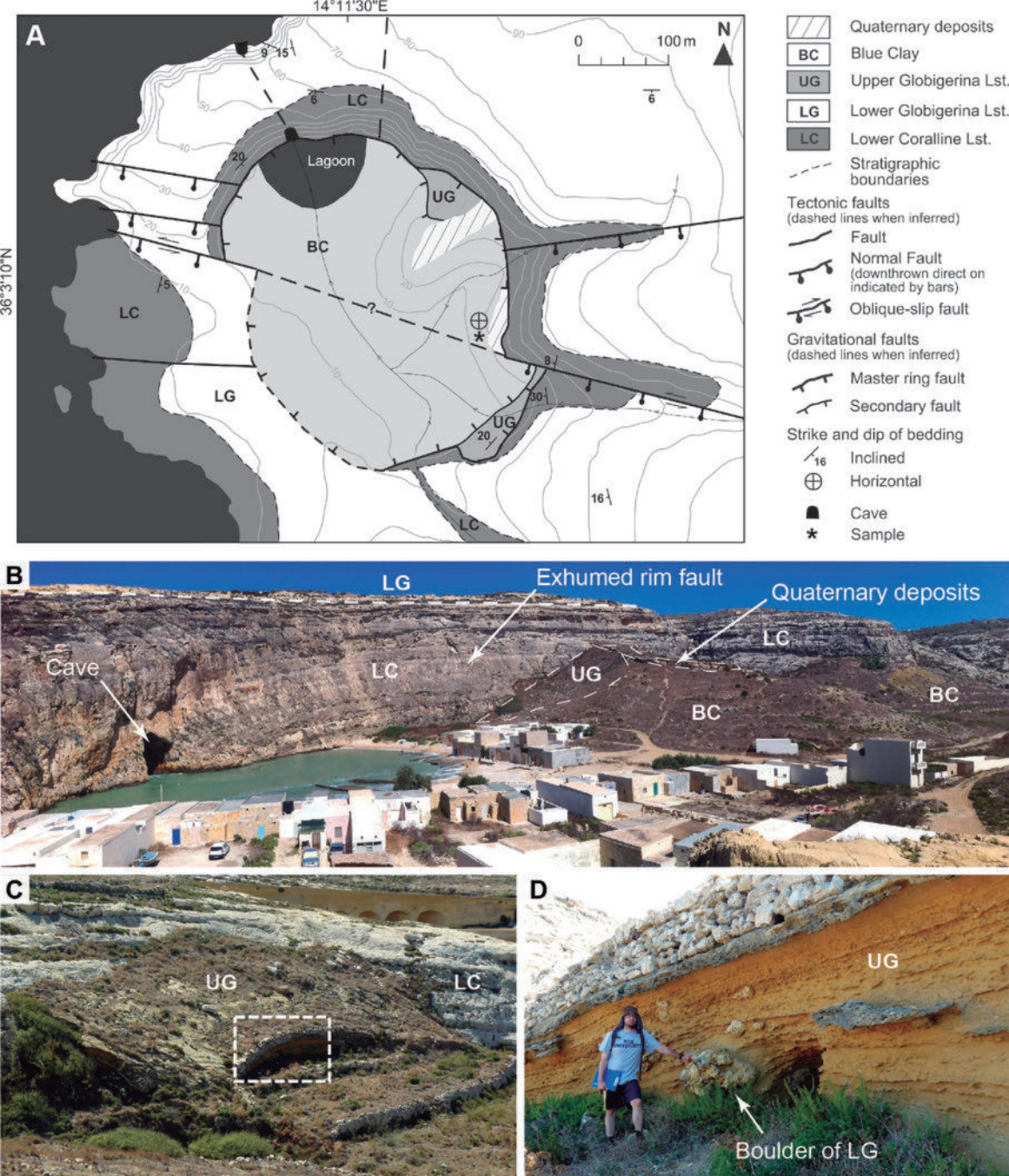
14°11'30"E
36°3'10"N
A
N
0
100 m
Lagoon
LC
UG
BC
LG
?
Quaternary deposits
Blue Clay
Upper Globigerina Lst.
Lower Globigerina Lst.
Lower Coralline Lst.
Stratigraphic boundaries
Tectonic faults
(dashed lines when inferred)
Fault
Normal Fault
(downthrown direct on indicated by bars)
Oblique-slip fault
Gravitational faults
(dashed lines when inferred)
Master ring fault
Secondary fault
Strike and dip of bedding
Inclined
Horizontal
Cave
Sample
B
Exhumed rim fault
Quaternary deposits
Cave
C
D
Boulder of LG

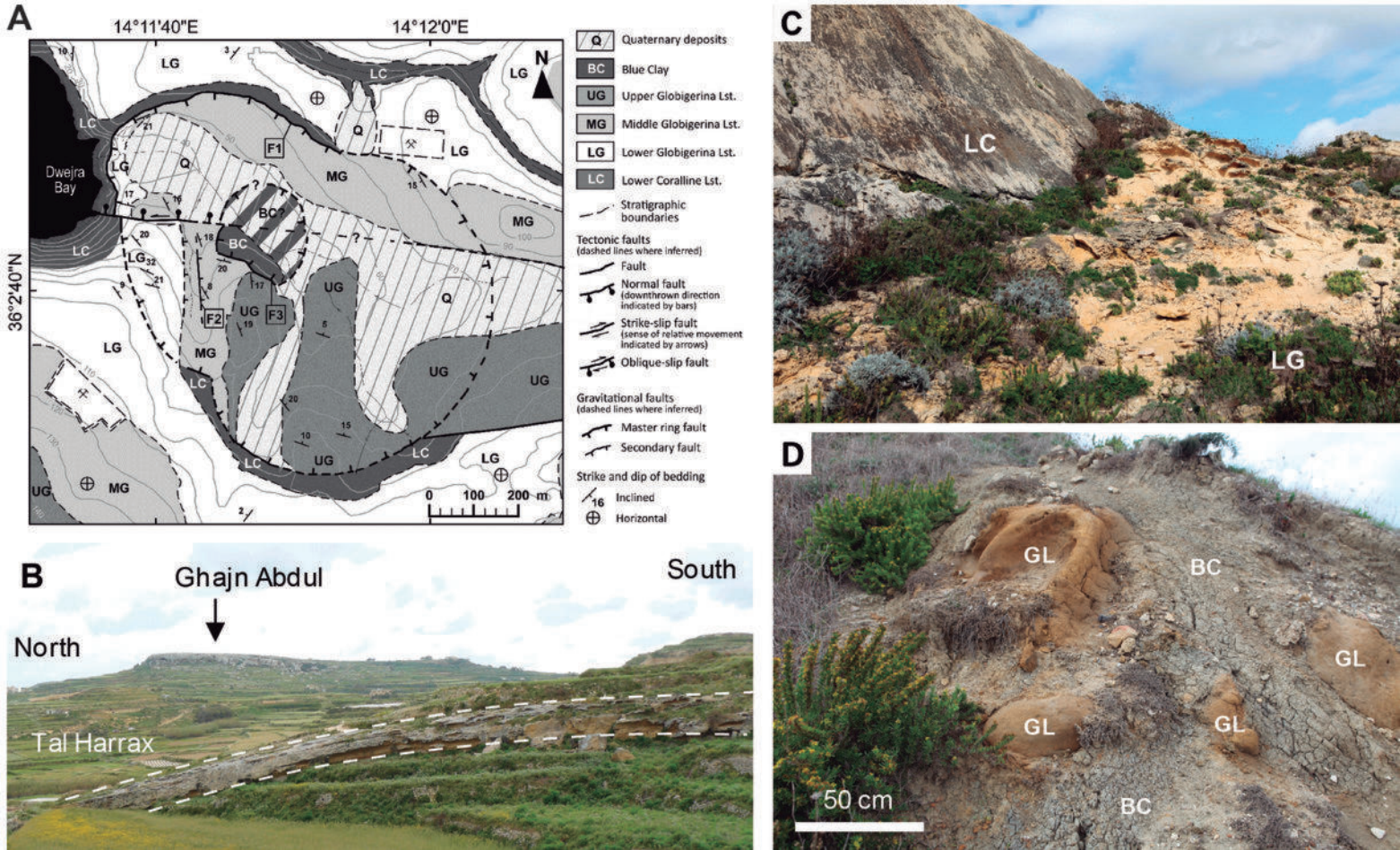
A
14°11'40"E
14°12'0"E
36°2'40"N
N
Dwejra Bay
F1
F2
F3
BC?
0 100 200 m
Q Quaternary deposits
BC Blue Clay
UG Upper Globigerina Lst.
MG Middle Globigerina Lst.
LG Lower Globigerina Lst.
LC Lower Coralline Lst.
Stratigraphic boundaries
Tectonic faults
(dashed lines where inferred)
Fault
Normal fault
(downthrown direction indicated by bars)
Strike-slip fault
(sense of relative movement indicated by arrows)
Oblique-slip fault
Gravitational faults
(dashed lines where inferred)
Master ring fault
Secondary fault
Strike and dip of bedding
Inclined
Horizontal
B
Ghajn Abdul
South
North
Tal Harrax
C
LC
LG
D
GL
BC
GL
GL
GL
50 cm
BC

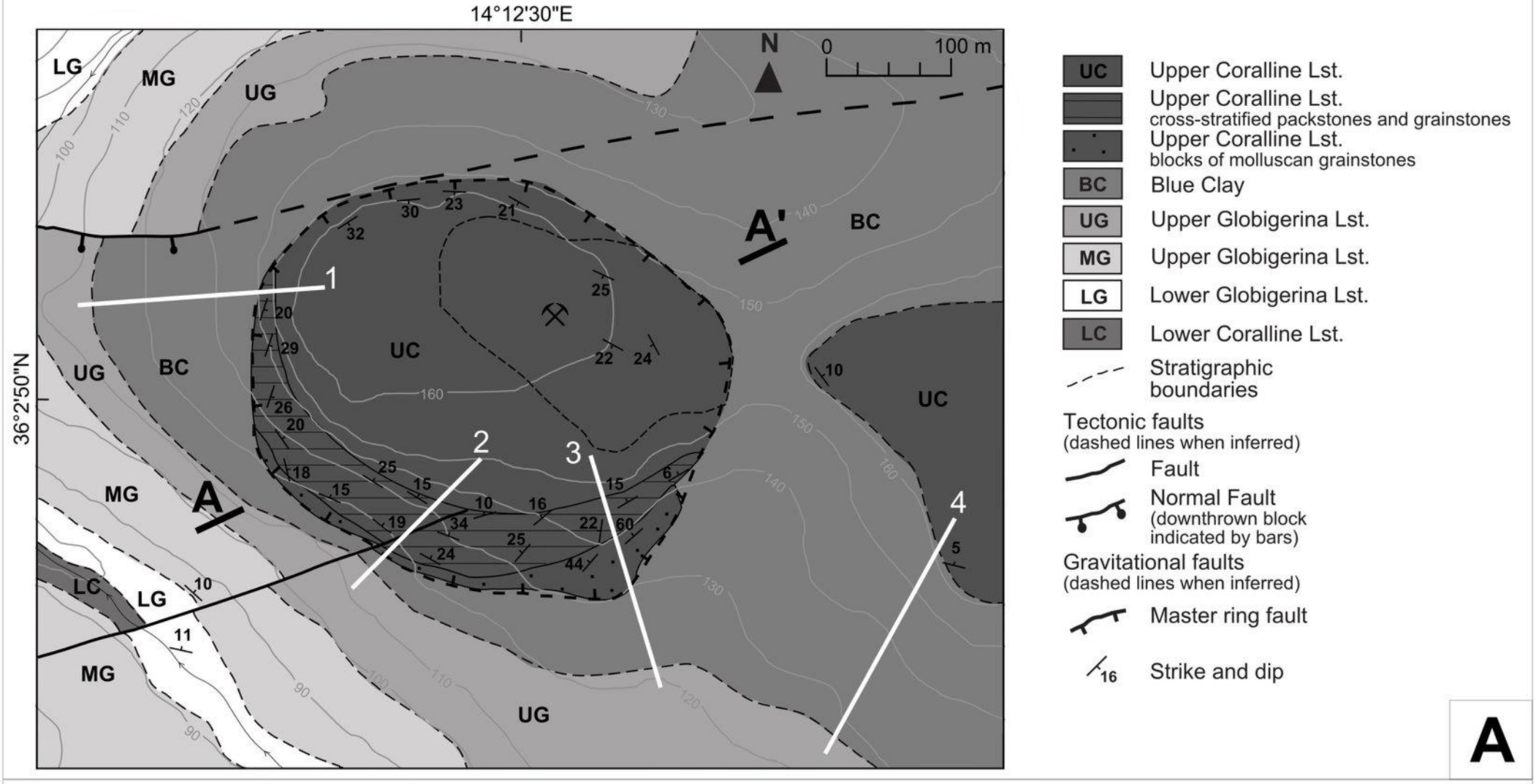
14°12'30"E
36°2'50"N
N
0
100 m
LG
MG
UG
BC
UC
LC
A
A'
1
2
3
4
Upper Coralline Lst.
Upper Coralline Lst.
cross-stratified packstones and grainstones
Upper Coralline Lst.
blocks of molluscan grainstones
Blue Clay
Upper Globigerina Lst.
Upper Globigerina Lst.
Lower Globigerina Lst.
Lower Coralline Lst.
Stratigraphic boundaries
Tectonic faults
(dashed lines when inferred)
Fault
Normal Fault
(downthrown block indicated by bars)
Gravitational faults
(dashed lines when inferred)
Master ring fault
Strike and dip
A

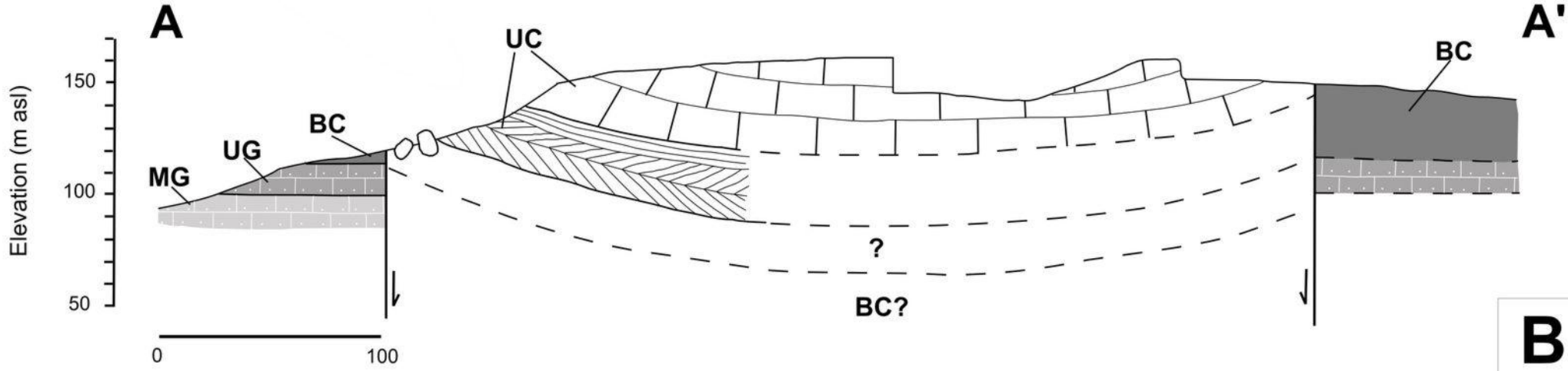
A
A'
Elevation (m asl)
150
100
50
0
100
UC
BC
UG
MG
?
BC?
B

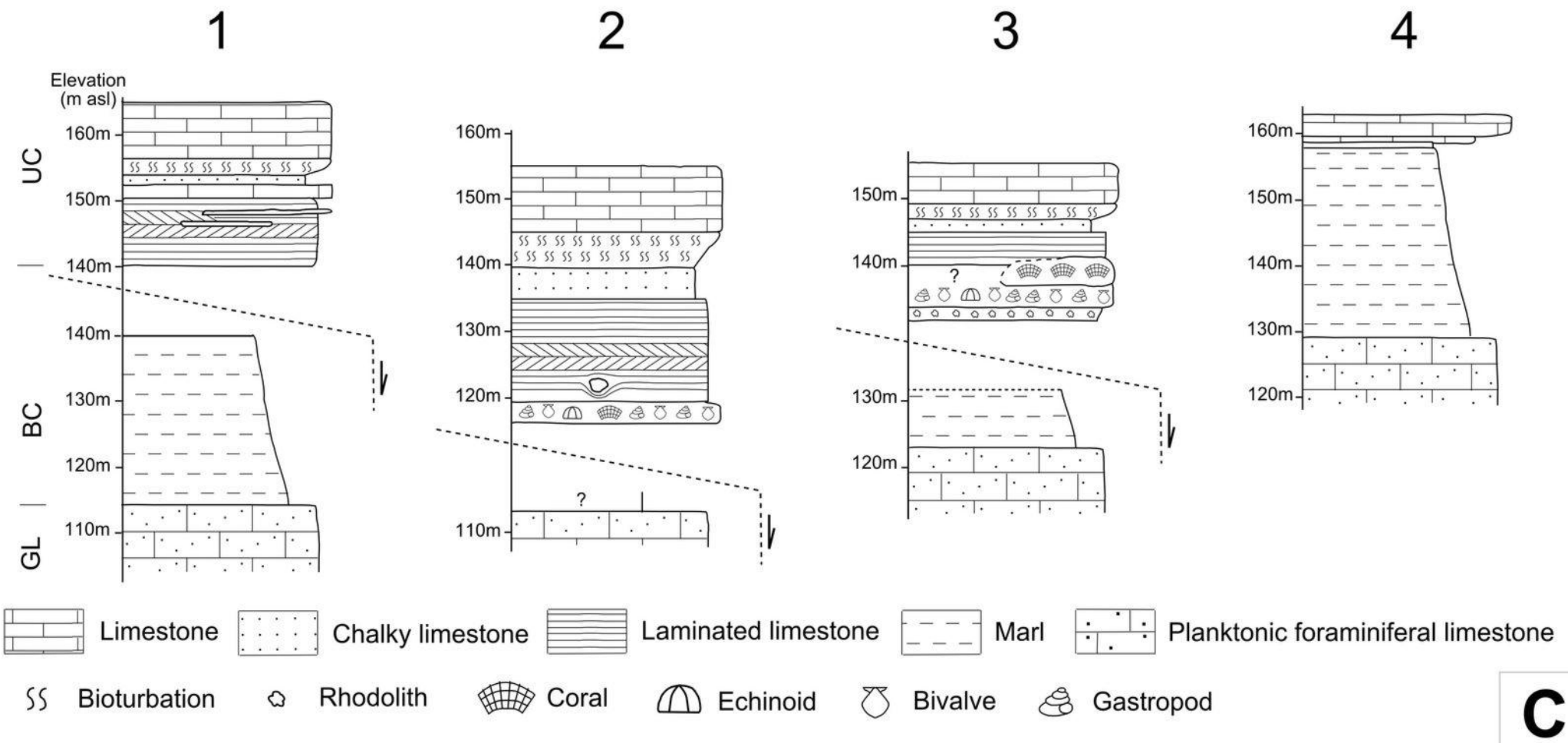
1
2
3
4
Elevation
(m asl)
160m
150m
140m
130m
120m
110m
UC
BC
GL
Limestone
Chalky limestone
Laminated limestone
Marl
Planktonic foraminiferal limestone
Bioturbation
Rhodolith
Coral
Echinoid
Bivalve
Gastropod
C

0 100 m

N

Hillshade derived from a LiDAR DEM

Dwejra North Bay

Dwejra Bay

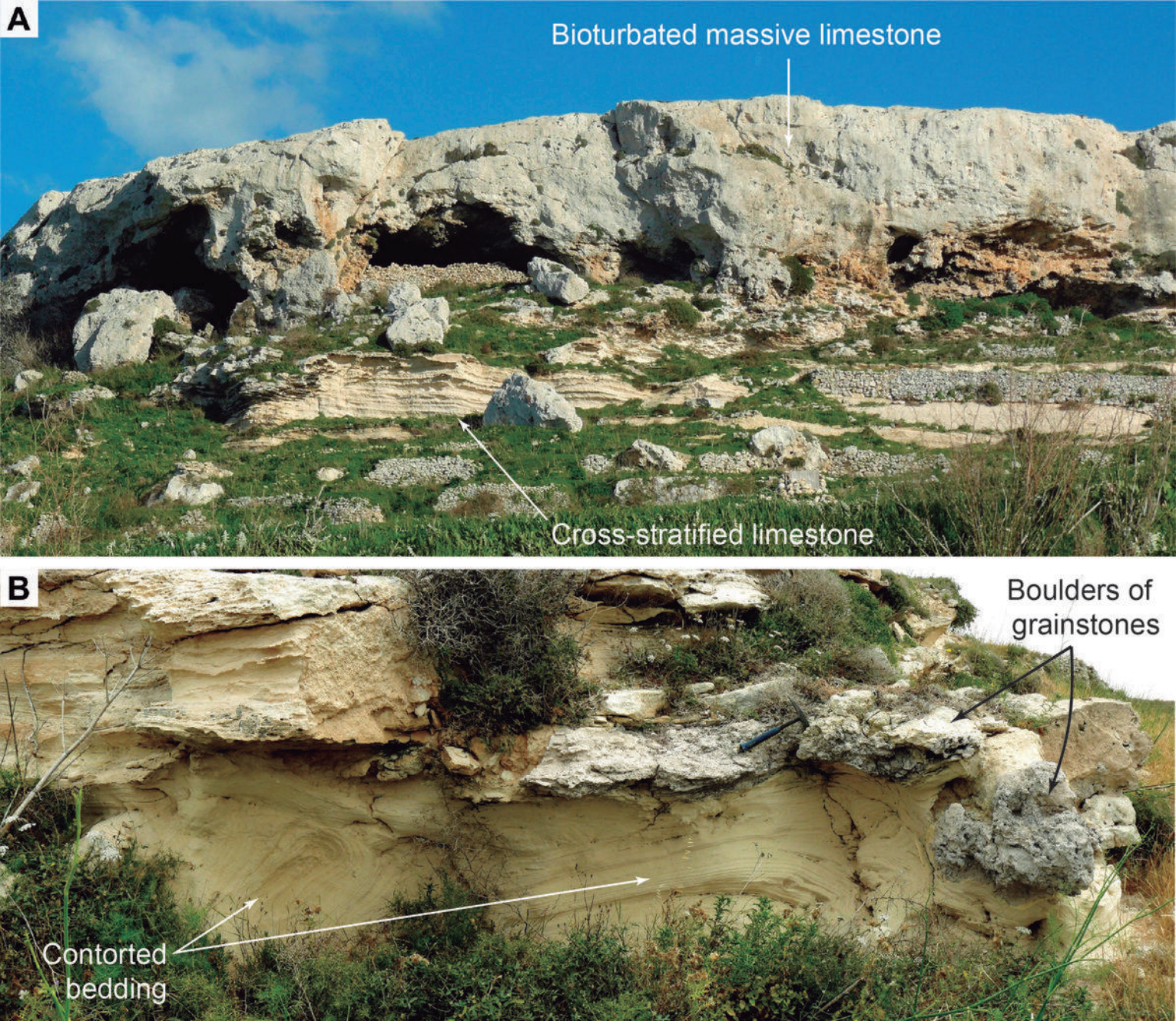
A
Bioturbated massive limestone
Cross-stratified limestone
B
Boulders of grainstones
Contorted bedding

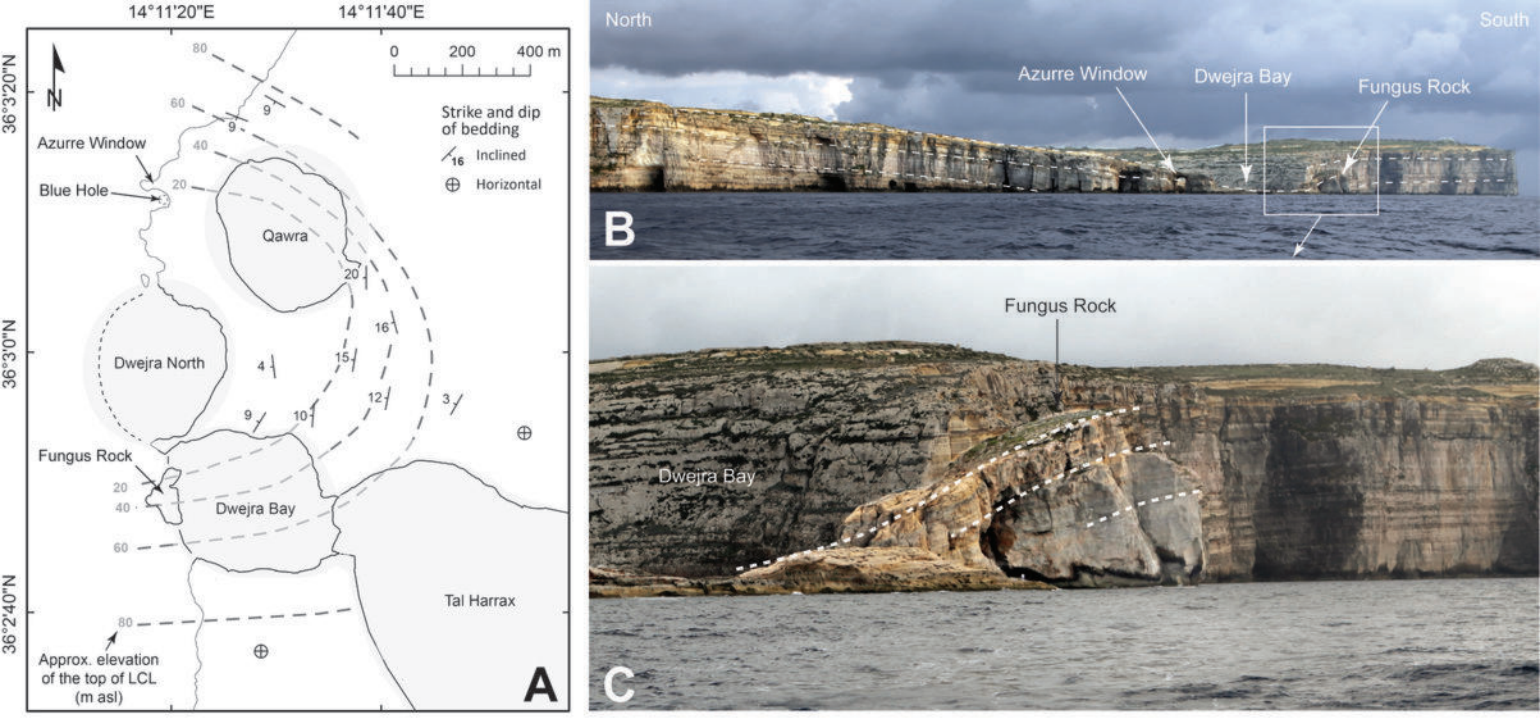
14°11'20"E
14°11'40"E
36°3'20"N
36°3'0"N
36°2'40"N
0 200 400 m
N
Strike and dip of bedding
16 Inclined
Horizontal
Azurre Window
Blue Hole
Qawra
Dwejra North
Fungus Rock
Dwejra Bay
Tal Harrax
Approx. elevation of the top of LCL (m asl)
A
North
South
Azurre Window
Dwejra Bay
Fungus Rock
B
Fungus Rock
Dwejra Bay
C

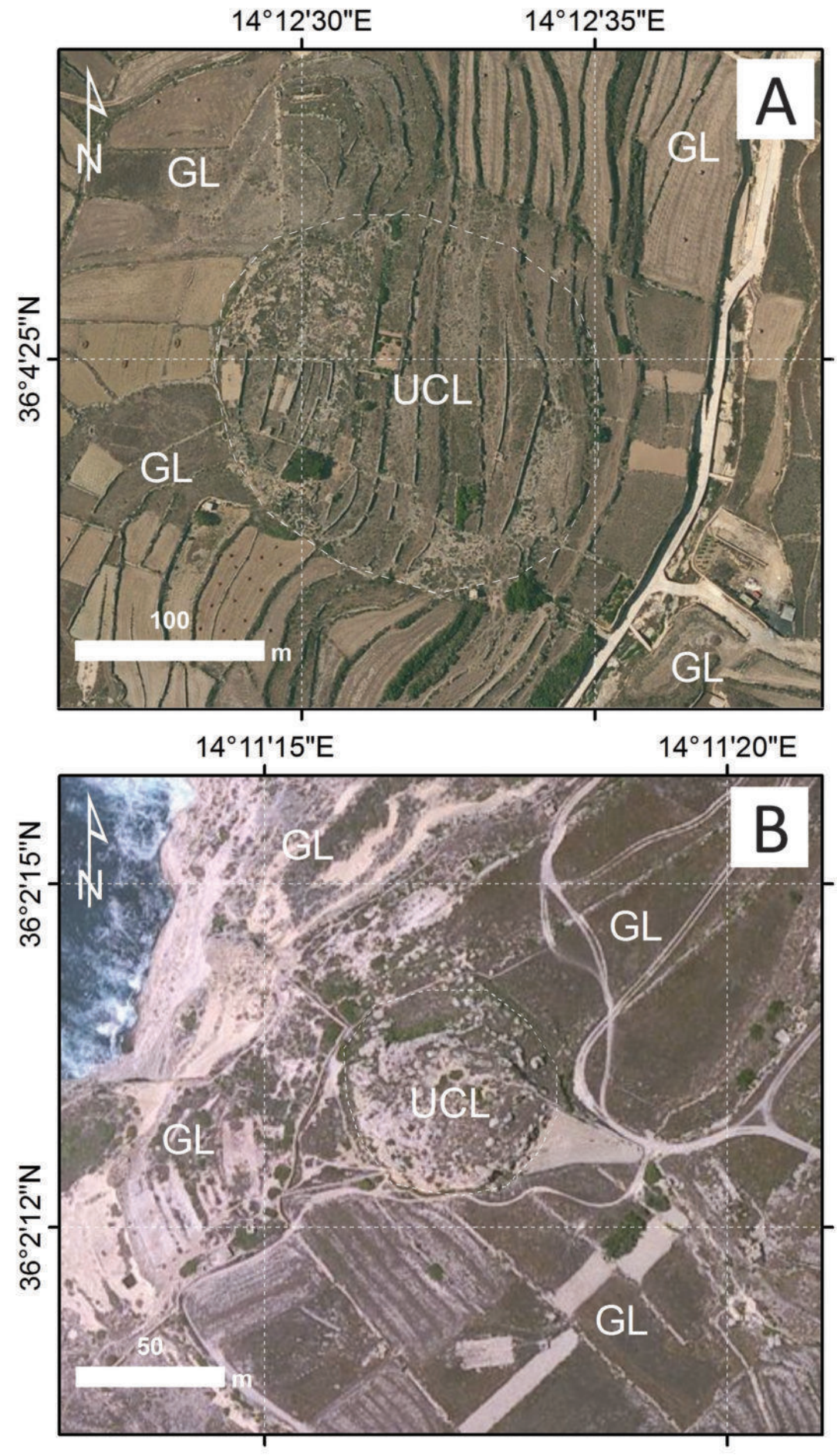
14°12'30"E
14°12'35"E
A
N
GL
GL
UCL
GL
GL
100
m
36°4'25"N
14°11'15"E
14°11'20"E
B
N
GL
GL
UCL
GL
GL
50
m
36°2'15"N
36°2'12"N